Chapter 9
Fiber Reinforced Composites with Cementitious (Inorganic) Matrix

Christian Carloni, Dionysios A. Bournas, Francesca G. Carozzi, Tommaso D'Antino, Giulia Fava, Francesco Focacci, Giorgio Giacomin, Giovanni Mantegazza, Carlo Pellegrino, Carlo Perinelli and Carlo Poggi

Abstract Fibre reinforced composite systems are increasingly used in civil engineering infrastructure applications for strengthening and rehabilitation of reinforced concrete (RC) structures. Composite materials represent a sustainable alternative to new construction because they allow for an extension of the original service life and therefore prevent demolition of existing structures. Promising newly-developed types of matrix that potentially represent a valid, sustainable, and durable alternative to epoxy, employed in fibre-reinforced polymer (FRP) composites, are the so-called inorganic matrices. Within the broad category of inorganic matrices, cement-based mortars have raised some interest in recent years. This chapter intends to highlight the potentials of this new category of fibre-reinforced composites as a viable alternative to traditional FRP systems. The latest advancements in this field and the new challenges that researchers will face in the future are presented and discussed.

Keywords FRCM · Strengthening · Cementitious matrix · Reinforced concrete

C. Carloni (✉)
University of Bologna, Bologna, Italy
e-mail: christian.carloni@unibo.it

D.A. Bournas · G. Giacomin
University of Nottingham, Nottingham, UK

F.G. Carozzi · G. Fava · C. Poggi
Politecnico of Milan, Milan, Italy

T. D'Antino · C. Pellegrino
Univeristy of Padua, Padua, Italy

F. Focacci
Univeristy eCampus, Novedrate, Italy

C. Perinelli
G&P Intech Srl, Altavilla Vicentina, Italy

G. Mantegazza
Ruredil Spa, San Donato Milanese, Italy

C. Pellegrino and J. Sena-Cruz (eds.), *Design Procedures for the Use of Composites in Strengthening of Reinforced Concrete Structures*, RILEM State-of-the-Art Reports 19, DOI 10.1007/978-94-017-7336-2_9

Introduction

Strengthening and rehabilitation of reinforced concrete (RC) structures with externally-bonded composite materials represent a sustainable alternative to new construction because they allow for an extension of the original service life and therefore prevent demolition of existing structures. In the last two decades fibre-reinforced polymer (FRP) composites have been the most common type of composite used for structural applications. FRP comprises of continuous fibres (usually carbon, glass, or aramid) and a thermosetting (organic) resin, typically epoxy, as the matrix. Promising newly-developed types of matrix that potentially represent a valid, sustainable, and durable alternative to epoxy are the so-called inorganic matrices. Within the broad category of inorganic matrices, polymer-modified cement-based mortars have raised some interest in recent years. Composite materials that employ modified cement-based mortars are usually referred to as fibre-reinforced cementitious matrix (FRCM) composites. Alternative names have been proposed in the literature and refer to different types of matrix or application. Among the others, the most common names are TRM (Textile Reinforced Mortar) (e.g. Bisby et al. 2009; Triantafillou 2010), TRC (Textile Reinforced Concrete) (e.g. Banholzer et al. 2006; Brückner et al. 2006; Hartig et al. 2008; Hegger et al. 2006; Peled et al. 2008; Wiberg 2003; Zastrau et al. 2008), MBC (Mineral Based Composites) (Täljsten and Blanksvärd 2007) or FRC (Fiber Reinforced Cement) (e.g. Wu and Sun 2005). Similar materials used for masonry structures strengthening applications are identified in the technical literature with the acronyms CMG (Cementitious Matrix-Grid system) (Prota et al. 2006; Lignola et al. 2009), IMG (Inorganic Matrix Grid system) (Parisi et al. 2011), CFCM (Carbon Fiber Cement Matrix) (Kolsch 1998). FRCM is used as the acronym of fabric reinforced cementitious matrix in the ACI guideline (ACI 2013). In the following sections the acronyms FRCM as well as TRM will be used as synonyms to refer to composites that employ inorganic matrices.

In FRCM composites, fibres are typically bundled (rovings), and the fibre pattern can be modified from unidirectional to bidirectional textile weaves or fabrics in an attempt to improve the bond characteristics. The still-limited available literature reports that FRCM composites can be used effectively for strengthening and rehabilitation of RC structures. In FRP-concrete joints, it is well-understood that interfacial crack propagation typically occurs within a thin layer of the substrate close to the FRP composite, and therefore the concrete mechanical and fracture properties and the surface treatment play a fundamental role in the evaluation of the strengthening performance. In FRCM-concrete joints the interfacial debonding might occur within the composite for some commercially available FRCM systems; hence the substrate, on which the composite is applied, may not play a key role in the design of the strengthening system, which is an interesting aspect of this composite. Large slips at the interface between fibres and matrix have been observed during the debonding of FRCM composites from a concrete substrate (D'Ambrisi et al. 2012, 2013a; D'Antino et al. 2014; Sneed et al. 2014; Carloni

et al. 2014). When the debonding occurs at the matrix-fibre interface, the phenomenon itself is complicated by the telescopic behaviour observed among the fibre filaments of a fibre bundle where the core filaments have a different mechanism of stress transfer with respect to the outer filaments, mainly due to the different impregnation of the fibres by the matrix. Although real applications of FRCM composites on structure subjected to fatigue loading were performed (D'Ambrisi et al. 2015), studies regarding the behavior of FRCM composites subjected to fatigue loading are very limited (D'Antino et al. 2015).

In the next section a brief description of some of the FRCM systems commercially available is presented to show the great variability of the matrix-fibre combinations, which in turn determines also a variability of the response of the FRCM-concrete interface. After a brief presentation of the available FRCM systems, the tensile behaviour, the bond characteristics, and finally the use of FRCM systems for flexural and confinement applications are presented.

FRCM Materials

In this section a brief description of some of the commercially available FRCM systems is reported.

Materials by G&P

G&P introduced in the international market different composite systems such as FRCM (carbon, AR glass and basalt grids) and SRG (UHTSS high resistance steel fabric) used with inorganic matrix (like cementitious or structural lime) for structural reinforcement of buildings. The main advantages of these systems are fire resistance, easy application on rough and moist surfaces, and ductility. In addition, FRCM and SRG systems are also compatible with historical buildings and monuments.

The main applications of FRCM and SRG systems are in the following areas:

- Restoration of historical buildings and particularly the reinforcement of masonry structures such as walls, arches, vaults, and domes. In this case it is important to highlight that these systems are highly compatible with the historical masonries also when there are frescoes on the opposite surface of application.
- Improvement of structures in seismic areas with increase of strength and ductility of masonry and reinforced concrete elements.
- Reinforcement of tunnels and structures which need high fire resistance.

The fibres employed are obtained with carbon, glass, basalt grids, and steel fabric with the following mechanical properties.

- Carbon grid uni-bi directional C-NET (filament)
  - Weight g/m^2 100–170–200–220
  - Elastic modulus GPa 240
  - Tensile strength MPa >4500
  - Strain at failure % >1.5
- AR Glass grid bidirectional G-NET (filament)
  - Weight g/m^2 120–250–320
  - Elastic modulus GPa 65–74
  - Tensile strength MPa >3000
  - Strain at failure % >3
- Basalt grid bidirectional B-NET (filament)
  - Weight g/m^2 250–350
  - Elastic modulus GPa 90
  - Tensile strength MPa >3200
  - Strain at failure % >3
- Steel fabric UHTSS unidirectional STEEL NET

TYPE		150	190
– Weight	g/m^2	1528	1910
– Elastic modulus	GPa	190	190
– Tensile strength	MPa	3345	3345
– Strain at failure	%	>2.2	>2.2

The following inorganic matrices are technically approved and certified to be used with carbon, glass, and basalt grids and steel fabrics.

- CONCRETE ROCK W cementitious mortar with reactive nano compound additives specific for low thickness, no-shrinking, sulphates resistant.
- CONCRETE ROCK V-V2 cementitious mortar, one or two components, no-shrinking, with high resistance for concrete repair.
- LIMECRETE lime hydraulic mortar, with high resistance and adhesion to the support for masonry and historical buildings.
- LIMECRETE FR lime hydraulic mortar for low thickness, with high resistance and adhesion to the support for masonry and historical buildings.

FRCM Materials by Ruredil

The FRCM system patented by Ruredil worldwide features the following advantages:

- high heat resistance: once the matrix has hardened, the system is not affected by the outdoor temperature.

- excellent reaction to fire: the system reacts in the same way as the substrate, because the inorganic matrix maintains its properties up to a temperature of 550 °C, is not combustible, emits very little smoke and does release off incandescent particles;
- high durability even under damp conditions.
- effective even if applied over a damp substrate: humidity promotes adhesion to the hydraulic matrix, whereas it reduces the adhesion of inorganic resins to the substrate;
- easy handling: inorganic matrix is prepared in the same way as any hydraulic product;
- applicable even on rough, irregular surfaces: does not require preliminary smoothing of the surface;
- applicable under a great variety of environmental conditions;
- non-toxicity of the matrices employed for workers and the environment: they may in fact be considered similar to a traditional inorganic mortar.
- easy cleaning of utensils: water is sufficient, with no need for the solvents required to clean off resins, which are harmful to human health and the environment.

This breakthrough technology has resulted in a product line that has obtained certification from ICC Evaluation Services (ICC-ES) according to AC434-13 (2013). AC434-13 establishes guidelines for the necessary tests and calculations required to receive a product research report from ICC-ES. Thus, this product can now be accepted by code officials under Section 104.11.1 of the International Building Code, which allows research reports to be used as a source of information to show building code compliance of alternative materials. Example of applications with PBO and Carbon FRCM materials by Ruredil are shown in Figs. 9.1 and 9.2, respectively.

Fig. 9.1. Structural retrofitting of cooling towers with PBO-FRCM (by Ruredil): **a** Power plant cooling tower. **b** and **c** application of the FRCM composite

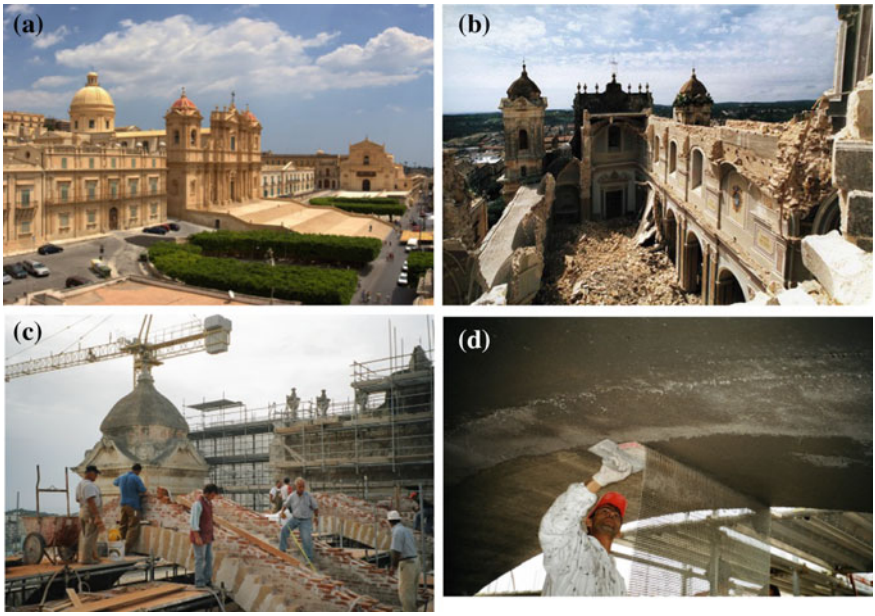

Fig. 9.2 Reconstruction and seismic retrofitting of the Cathedral Church of Noto (Italy) using C-FRCM (by Ruredil): **a** The Cathedral (today) Noto, Siracusa Italy; **b** the collapse of the structure due to earthquake; **c** and **d** reconstruction and seimic retrofitting of the arches of the main nave

Mechanical Characterization of FRCM Systems: Tensile Test

This section reports a summary of the experimental work, carried out at the Politecnico di Milano and University of Padova, to characterize FRCM composites in tension.

Finding a reliable and shared experimental procedure to test FRCM composites in tension is of particular importance due to the great number of materials and fibre-matrix combination available. The scientific literature reports several difficulties in characterizing the performance of FRCM composite. Different test setups have been used and, although some authors already proposed some recommendations, a shared test procedure has not been published yet (Hartig et al. 2012; Häußler-Combe and Hartig 2007; Jesse et al. 2005, 2009). The response of FRCM composites in tension may be influenced by: specimen production, dimensions, and shape, and load application. Hartig et al. (2012) classified two types of load application: "rigid load application" in which the main transfer mechanism between specimen and clamping is adhesive tension and shear; and "soft clamping" with friction load transfer allowing for gradual load application. There are different procedures to analyse the deformations (Contamine et al. 2011): (a) displacements of the clamps testing machine; (b) strain gauges, that could be inadequate in the

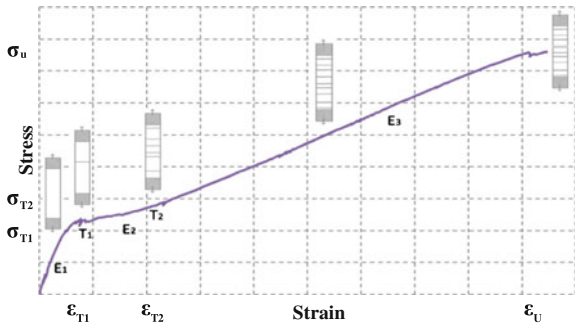

Fig. 9.3 Stress–strain behavior of a FRCM composite subject to tensile test

case of multi-cracking behaviour; (c) LVDT displacement transducers. The deformations are measured using an extensometer which analyses a length equal to the 30 % of the total specimen length, and compared with the ratio between the displacement of the tensile machine clamps and the length of the specimens.

The characteristic behaviour of FRCM materials under tension can be considered tri-linear. The first branch represents the uncracked state, where the slope of the stress–strain curve reflects the elastic modulus of the matrix. The second branch corresponds to the crack-formation: in this state several cracks gradually form due to the increase in the tensile stress applied. The length and smoothness of this portion of the curve depend on the quality of the bond between the fibres and matrix and the volume proportion of fibres in the composite activated by load transfer. The third branch represents the crack-widening. In this region only few new cracks appear and the existing cracks become wider. The specimen fails when the tensile strength of the fibres is reached. In the third region the slope reflects the elastic modulus of the dry fibres. Figure 9.3 shows the different phases of the stress-strain curve, the cracking of the specimens, and the failure mode.

The main parameters that could be analysed are:

- tensile stress and strain in the transition point between two phases (point T_1 and T_2), σ_{T1}, σ_{T2}, ε_{T1}, ε_{T2}
- elastic modulus of the three phases, E_1, E_2, E_3
- ultimate tensile stress and strain, ε_u, σ_u

In the first phase, the tensile stress is calculated by dividing the applied load by the area of the FRCM coupon in order to compare the elastic modulus with the one of the mortar, and the stress (σ_{T1}) of the uncracked mortar with the maximum tensile stress of the mortar. In the third phase, the elastic modulus and the maximum stress are computed with respect to the area of the longitudinal fibres.

Characteristic Behavior of FRCM Materials Under Tension (Politecnico di Milano)

Test results of tensile tests herein presented were defined in accordance with AC434 (2013) and the acceptance criteria for FRCM composites outlined in the draft of the Italian guidelines, which are yet to be published.

Tensile coupons are usually made in a flat mold by applying a first layer of cementitious mortar (approximately 4–5 mm), a layer of the fibre mesh which is evenly wetted with the fresh material, and a second layer of the cementitious mortar. The coupons should be cured for 28 days. The dimensions of the tensile coupons were 400 mm (length) × 40 mm (width) × 10 mm (thickness) (Fig. 9.4). During the curing phase attention should be paid to the possibility that some micro-cracks develop due to non-homogeneous shrinkage. Micro-cracking, a non-perfect planarity in the sample, and a non-constant thickness could have great influence on the test results.

At the ends of the samples FRP tabs of glass or carbon fibres were bonded in order to have a good stress distribution during the test and to avoid damages in the sample. Three different FRCM materials are presented as an example of material characterization via tensile test: FRCM with a mesh in poliparaphenylene benzobisoxazole fibres (PBO-FRCM), a mesh in carbon fibres (C-FRCM) and a mesh in glass fibres (G-FRCM).

Tensile tests were carried out with a testing machine with capacity of 100 kN under displacement control at an initial rate equal to 0.3 mm/min. The rate was increased to 0.5 mm/min after the first cracking phase. Axial strain was measured using an extensometer with a gauge length (between 100 and 200 mm) greater than 30 % of the total specimen length. The strain measured was then compared with the one obtained by dividing the stroke of the testing machine by the length of the specimens.

The tensile tests on PBO-FRCM coupons were characterized by a tri-linear behaviour; the results presented a large variability, in particular in the values corresponding to the point between the first and the second branch (T_1) and between the second and the third branch (T_2). This phenomenon is due to the non-constant dimension of the specimen section and to the first crack location with respect to the extensometer. The results showed a similarity between the stress in the mortar at point T_1, when the first crack appeared (3.5 MPa), and the tensile strength of the mortar defined by an indirect tensile test (4.7 MPa). The elastic modulus of the first branch corresponded to the one of the mortar. The elastic modulus of the third phase (218 GPa) was comparable with the elastic modulus of the dry PBO mesh (216 GPa) obtained from a tensile test on dry PBO rovings.

Tensile tests on G-FRCM coupons were characterized by a tri-linear behaviour in which it could be difficult to distinguish the second and third phase. The elastic modulus of the last branch (57 GPa) could be compared with the elastic modulus of the glass fibre grid (55 GPa).

In Fig. 9.5 a comparison between the results on the different materials is shown (Carozzi and Poggi 2015).

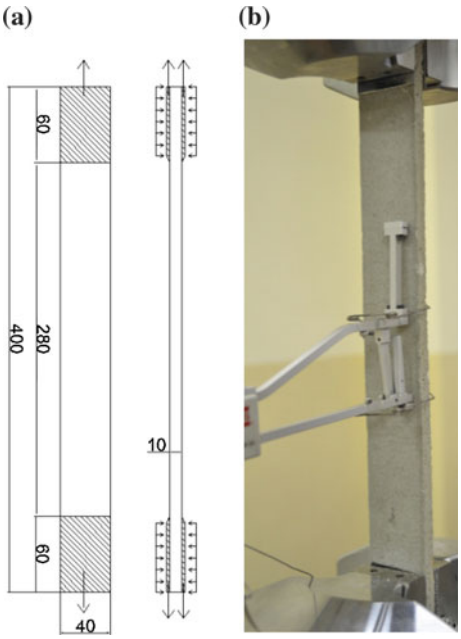

Fig. 9.4 **a** Specimens size. **b** Tensile test set-up

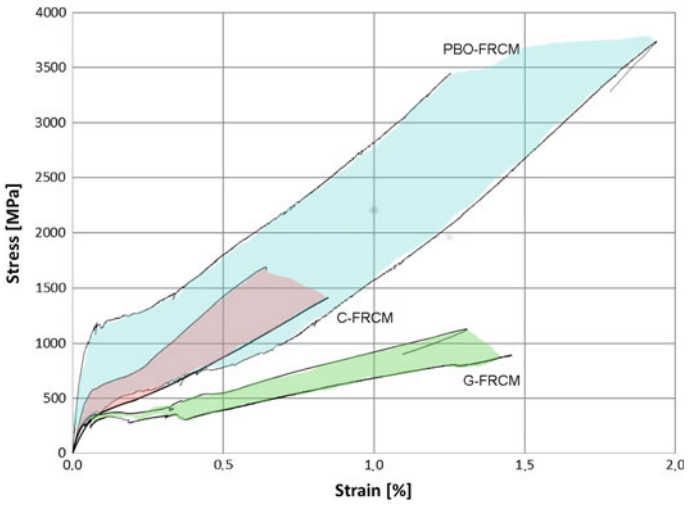

Fig. 9.5 Tensile tests results

Tensile tests on C-FRCM showed a tri-linear behaviour. Slippage was observed in many tests due to issues with bond and impregnation between the mortar and the dry carbon fibres. For this reason the elastic modulus of the third phase (191 GPa) could not be compared with the elastic modulus of the dry carbon textile (200 GPa).

Experimental Test to Characterize FRCM Composites (University of Padova)

The test procedure suggested by Hartig et al. (2007) and Jesse et al. (2009) was adopted by Pellegrino and D'Antino (2013) to characterize the overall behaviour of two different FRCM composites. The results obtained are here briefly revisited and commented on.

The specimens tested were comprised of a polymer-modified cementitious matrix used to embed a carbon fibre net and a steel fibre net. The carbon fibre net was comprised of longitudinal and transversal bundles with a width of approximately 5 mm each. The steel fibre net was comprised of longitudinal steel strands with diameter of approximately 0.48 mm^2 each, held together through a plastic fibre net. The same cementitious matrix was used both the carbon and steel fibre nets. The matrix was characterized in compression and bending according to the European Standard UNI EN 1015-11 (2007). Nine matrix prisms with dimensions 40 mm × 40 mm × 160 mm were cast from the same batch used to cast the FRCM tensile test specimens and were tested under bending and compression. The mean value of the flexural strength was $f_{flex} = 5.0$ MPa whereas the mean value of the compressive strength was $f_{c,matrix} = 39.3$ MPa. The mechanical characteristics of the carbon net were provided by the manufacturer. The elastic modulus, tensile strength, and tensile strain were $E_f = 240$ GPa, $f_f = 3800$ MPa, and $\varepsilon_f = 0.015$, respectively. The steel fibres were mechanically characterized by means of tensile tests. The indications of ASTM (1996) were used as base for the tests, which provided an average value of the tensile strength $f_{f,sf} = 3350$ MPa and a corresponding ultimate strain of $\varepsilon_{f,sf} = 0.0225$.

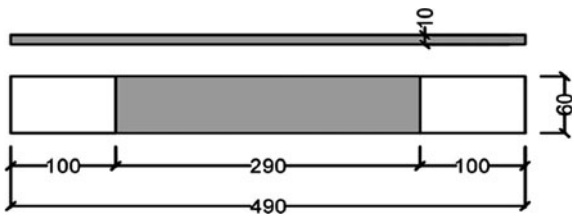

Fig. 9.6 FRCM specimen, dimension in mm

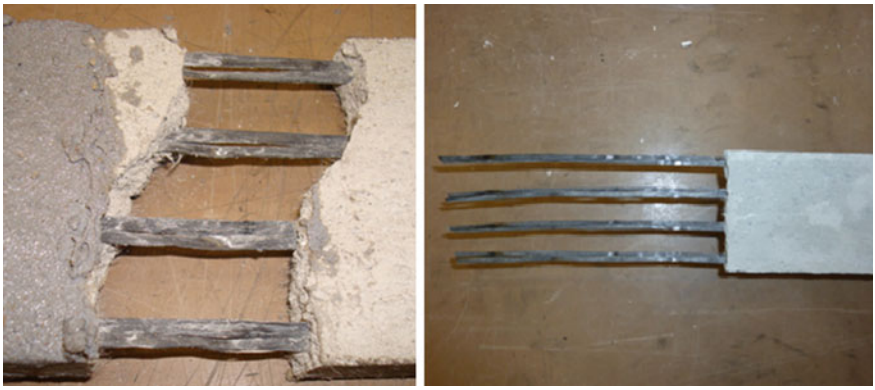

Fig. 9.7 Particulars of carbon FRCM specimens after failure

Twenty FRCM coupons, 10 with carbon fibres and 10 with steel fibres, were cast and tested in tension. The specimens were comprised of a fibre net ply embedded between two matrix layers that form a matrix prism (coupon) 490 mm long, 60 mm wide and 10 mm thick (Fig. 9.6).

In order to reduce the matrix roughness and avoid possible stress concentration, a thin layer of gypsum was applied at the ends of each specimen for a length approximately equal to 100 mm. Two steel plates, bolted together to assure uniform pressure on the clamped area of the specimen, were used to grip both ends. According to Hartig et al. (2012) a rubber layer was placed between the gypsum and the steel plates to avoid any possible local stress concentrations at the ends of the specimen. A DD1 strain transducer (gauge length = 100 mm) was applied at the centre of the specimen, and a load cell was used to record the load history.

The tests performed on carbon FRCM specimens did not provide significant results. Once the applied load reached the matrix tensile strength in one or more sections, the matrix cracked and the embedded fibres slid within the matrix without any increase of the tensile force (Fig. 9.7).

Although setup modifications were attempted in order to obtain a more effective clamping without inducing stress concentration, better results were not obtained. The failure mode observed may suggest that the length of clamping has to be properly designed but also that the surface treatment of the carbon fibres was not appropriate for this applications. Carbon fibres appeared smooth and clean after failure (Fig. 9.7), and this circumstance could indicate low bond properties between the fibres and the matrix. The results obtained from these tests indicate that the clamping system has to be properly designed and the surface treatment of the fibres has to be taken into account.

Steel fibres showed better adhesion to the cement-based matrix leading to good results, though complete failure of the composite due to steel rupture was not always reached. The opening of several transversal cracks in the cementitious matrix followed by the sudden failure of most of the steel strands was observed. During the tests, longitudinal splitting phenomena were also observed (Fig. 9.8).

Fig. 9.8 Cracking, splitting and failure of the steel FRCM specimens

This phenomenon can be due to the fact that, although the cementitious matrix and the steel net have been properly designed for FRCM applications, steel strands were very close to each other, and the matrix penetration through the fibres was probably limited. This suggests that the spacing between strands has to be increased to improve the tensile behaviour of the FRCM system. The average ultimate stress obtained from these tests was 3290 MPa, which is very close to that obtained with the tensile test on the bare fibres reported above. Although the results of the tests on steel FRCM specimens were acceptable results in terms of ultimate load, the strain transducer did not provide useful measurements since it was strongly disturbed by matrix crack growth and propagation at different cross sections.

The test setup adopted does not seem to be suitable to characterize the FRCM composites presented in this study since it did not provide any information on their behaviour but was only able to find the ultimate load in case of steel FRCM specimens. Further investigations are needed to find a reliable, repeatable, and effective experimental test setup to characterized FRCM composites.

Analysis of the FRCM-Concrete Bond Behaviour

This section report the main results of an extensive experimental campaign carried out on FRCM-concrete joints to study the stress-transfer mechanism between the concrete support and the strengthening composite. The FRCM employed was comprised of a polyparaphenylene benzobisoxazole (PBO) fibre net embedded within a polymer-modified cementitious matrix. The parameters varied were the composite bonded length and bonded width. In addition, strain gauges were applied to the fibre net to study the stress-transfer mechanism. The PBO FRCM-concrete joints showed in this section were tested using a single-lap direct-shear test set-up.

Results on PBO FRCM-concrete joints tested using a double-lap direct-shear test set-up can be found in Sneed et al. (2015).

Test Set-up and Material Characteristics

Eighty-two FRCM-concrete joint specimens, herein presented, were tested using the single-lap direct-shear test set-up. The classical push-pull configuration was adopted where the fibres were pulled while the concrete prism was restrained (Smith and Teng 2002; Subramaniam et al. 2007, 2011; Carloni and Subramaniam 2012; Carloni et al. 2013; D'Antino et al. 2013, 2014). Two different concrete prisms were used, both had the same cross Section (125 mm width × 125 mm depth), but different lengths (L = 375 mm or L = 510 mm). The faces of the concrete blocks were sandblasted prior to applying the first (internal) layer of matrix. The nominal width b^* and average thickness t^* of one longitudinal fibre bundle were 5 and 0.092 mm, respectively. The matrix was applied only in the bonded area to embed the fibres and bond the composite to the concrete substrate (Fig. 9.9). Fibres were bare outside the bonded area. A single layer of PBO fibre net was applied onto the internal matrix layer and the transversal fibre bundles, which were all on one side of the longitudinal fibre bundles, were placed against the internal layer of matrix for some specimens. A second (external) 4 mm layer of matrix was applied over the PBO fibre net. The matrix layers had a thickness of 4 mm each as per the manufacturer's recommendations. The bonded width (b_1) and length (ℓ) of the composite were varied. Two aluminium plates (Fig. 9.9) were attached with a thermosetting epoxy to the end of the fibre strip to improve gripping during testing.

The concrete prism was restrained against movement by a steel frame bolted to the testing machine base. The direct-shear tests were conducted under displacement control using a close-loop servo-hydraulic universal testing machine. Two linear variable displacement transducers (LVDTs) were mounted on the concrete surface

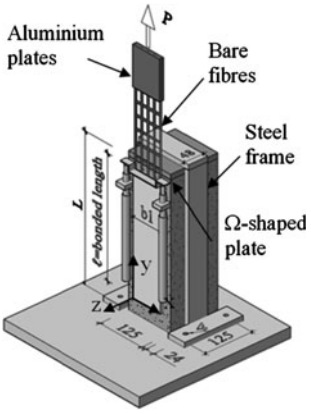

Fig. 9.9 Single-lap direct-shear test set-up

close to the edge of the composite bonded region. The LVDTs reacted off of a thin aluminium Ω shaped bent plate that was attached to the PBO transversal fibre bundle surface adjacent to the beginning of the bonded area (Fig. 9.9). The average of the two LVDT measurements, defined as the global slip g, was used to control the test with a constant rate of 0.00084 mm/s. The readings of the two LVDTs can be also used to study the distribution of the applied load among the width of the composite (Carloni et al. 2014). The applied load is termed P in this section.

From the same batch used to cast the concrete prisms, twelve (6 + 6) 100 mm × 200 mm cylinders were cast. Their average compressive strength (ASTM 2011a) and splitting tensile strength (ASTM 2011b) were 42.5 MPa (CoV = 0.013) and 3.4 MPa (CoV = 0.113) for the shorter blocks (L = 375 mm), and 33.5 MPa (CoV = 0.085) and 3.0 MPa (CoV = 0.042) for the longer blocks (L = 510 mm). At least two 50 mm × 100 mm cylinders were cast from each batch of matrix used to cast the FRCM composite. The average compressive (ASTM 2011a) and splitting tensile strengths (ASTM 2011b) of the matrix were 28.4 MPa (CoV = 0.092) and 3.5 MPa (CoV = 0.231), respectively. The bare PBO fibres were tested in tension as prescribed in ASTM (1996). The average measured tensile strength, ultimate strain, and elastic modulus were 3014 MPa (CoV = 0.068), 0.0145 (CoV = 0.104), and 206 GPa (CoV = 0.065), respectively.

Experimental Tests

The direct-shear test specimens were named following the notation DS_X_Y_S_D_Z^T, where X = bonded length (ℓ) in mm, Y = bonded width (b_1) in mm, S (if present) indicates that strain gauges were mounted on the specimen, D (if present) denotes that the specimen was tested until a constant load at the end of the test was measured, and Z = specimen number (Table 9.1). A superscript T after Z indicates that the fibre net was oriented with the transversal fibre bundles directly against the matrix internal layer. The peak load P^* of each specimens tested is reported in Table 9.1.

In order to compare specimens with different bonded widths, the ultimate stress σ^* is introduced in Eq. (9.1):

$$\sigma^* = \frac{P^*}{nt^*b^*} \tag{9.1}$$

where n is the number of longitudinal bundles.

All specimens reported in Table 9.1 failed due to debonding of the fibres within the embedding matrix. The debonding was associated with considerable slip of the fibres. For this reason, once the debonding initiates, the applied load is due to both the residual bond and the friction between fibres and matrix and between fibre filaments. When the fibres are completely debonded the applied load, which is due only to friction, remains constant ad the global slip increases. As an example, the

Table 9.1 Specimen tested in D'Antino et al. (2014)

Name	P^*(kN)	Name	P^*(kN)	Name	P^*(kN)
DS_100_34_1^T	1.92	DS_330_34_1^T	3.00	DS_330_80_2	8.84
DS_100_34_2^T	0.97	DS_330_34_2^T	3.51	DS_330_80_3	8.28
DS_100_34_3^T	1.62	DS_330_34_7	4.07	DS_330_80_D_1	8.90
DS_100_60_1	3.69	DS_330_34_8	4.02	DS_330_80_D_2	8.68
DS_100_60_2	3.83	DS_330_34_9	3.44	DS_330_80_D_3	8.90
DS_100_60_3	3.77	DS_330_43_1^T	4.43	DS_330_80_D_4	8.42
DS_150_34_1^T	2.22	DS_330_43_2^T	5.25	DS_330_80_D_5	8.58
DS_150_34_2^T	1.55	DS_330_43_3	5.27	DS_450_34_1	3.77
DS_150_34_3^T	2.87	DS_330_43_5	4.79	DS_450_34_2	3.85
DS_150_34_4^T	2.34	DS_330_43_6	5.09	DS_450_34_3	3.97
DS_150_60_1	5.25	DS_330_43_S_1^T	4.48	DS_450_60_1	6.40
DS_150_60_2	5.04	DS_330_43_S_2^T	5.12	DS_450_60_2	6.34
DS_150_60_3	3.05	DS_330_43_S_3^T	3.03	DS_450_60_3	6.44
DS_200_34_1	3.05	DS_330_43_S_5	4.03	DS_450_60_4	5.77
DS_200_34_2	2.52	DS_330_60_1^T	7.05	DS_450_60_5	6.51
DS_200_34_3	3.44	DS_330_60_2^T	6.56	DS_450_60_6	6.79
DS_200_60_2	5.66	DS_330_60_3^T	6.06	DS_450_60_7	6.65
DS_200_60_3	5.44	DS_330_60_4^T	6.50	DS_450_60_D_1	7.01
DS_200_60_4	6.58	DS_330_60_5^T	6.28	DS_450_60_D_2	6.67
DS_250_34_1^T	2.61	DS_330_60_6	7.01	DS_450_60_D_3	7.33
DS_250_34_2^T	2.11	DS_330_60_D_1	8.29	DS_450_60_S_1	6.63
DS_250_34_3^T	2.82	DS_330_60_D_2	7.12	DS_450_80_1	8.62
DS_250_34_4	3.21	DS_330_60_D_3	6.56	DS_450_80_2	9.07
DS_250_34_5	2.89	DS_330_60_D_4	5.24	DS_450_80_3	9.32
DS_250_34_6	3.61	DS_330_60_D_5	6.69	DS_450_80_4	8.86
DS_250_60_1	6.68	DS_330_60_S_1	6.30	DS_450_80_5	10.04
DS_250_60_2	6.17	DS_330_60_S_2	7.31		
DS_250_60_3	5.70	DS_330_80_1	8.47		

load responses of specimen DS_330_60_D_5, DS_330_80_D_1, and DS_450_60_D_1 are reported in Fig. 9.10.

It should be noted that some specimens, not reported in Table 9.1, failed due to fibre rupture outside the bonded area caused by the non-uniform distribution of the load among the different longitudinal bundles (D'Antino et al. 2014).

Effect of the Bonded Width

The effect of the bonded width on the behaviour of FRCM-concrete joints was investigated by comparing the ultimate stress σ^* with different composite bonded

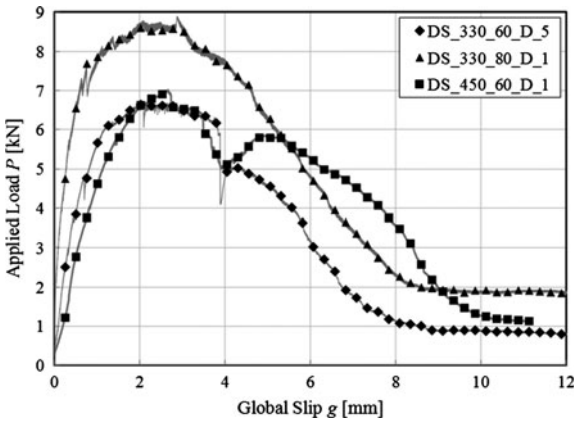

Fig. 9.10 Applied load P^* versus global slip g plot for specimens DS_330_60_D_5, DS_330_80_D_1, and DS_450_60_D_1

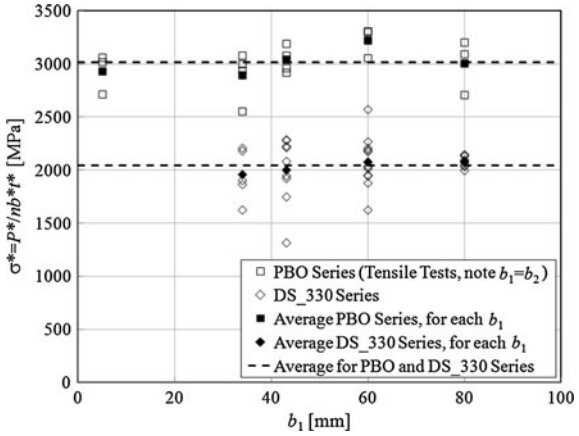

Fig. 9.11 Comparison of the ultimate stress σ^* versus bonded width b_1 for single-lap direct-shear tests (DS_330 Series) and tensile tests (PBO Series)

widths (b_1) for the test specimens with a bonded length ℓ = 330 mm. Figure 9.11 reports the variation of the σ^* for different widths in case of the direct-shear tests (DS_330 Series) and of the bare fibre tensile test (PBO Series). For each width the average value of the ultimate stress is reported with a black filled marker. The average values of the ultimate stress for all tensile tests and all single-lap shear tests plotted in Fig. 9.11 are reported with dashed lines. Although it is possible that a width effect exists considering a single bundle of fibres (Banholzer 2004), Fig. 9.11 suggests that a *global* width effect does not exist among multiple bundles and therefore for the entire width of the composite.

Strain Measurements

Nine specimens were instrumented with strain gauges applied directly to the central fiber bundle along the bonded length and to the central and edge fiber bundles outside the bonded area.

The axial strain profiles corresponding to different stages of the load response of specimen DS_330_43_S_5 are plotted in Fig. 9.12. The reference system is shown in Fig. 9.9. The load response of DS_330_43_S_5 is plotted in Fig. 9.13 to show the points corresponding to the strain profiles.

The strain profiles of Fig. 9.12 are similar to those obtained from direct-shear tests of the FRP-concrete interface (Carloni and Subramaniam 2012; Pellegrino et al. 2008), which suggests that a cohesive material interfacial law can be obtained for FRCM-concrete joints. In this study, the strain profiles obtained experimentally will be approximated by Eq. (9.2) (Carloni and Subramaniam 2012):

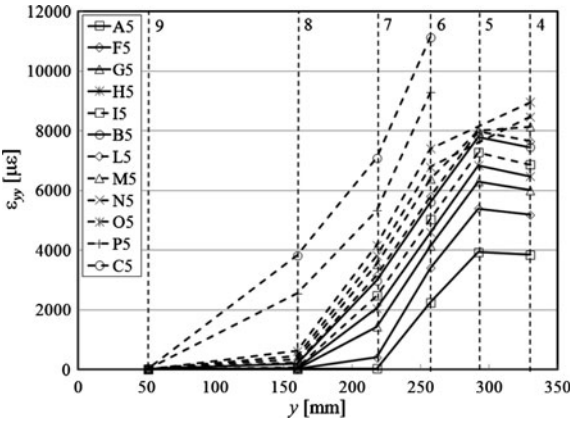

Fig. 9.12 Axial strain profile of specimen DS_330_43_S_5

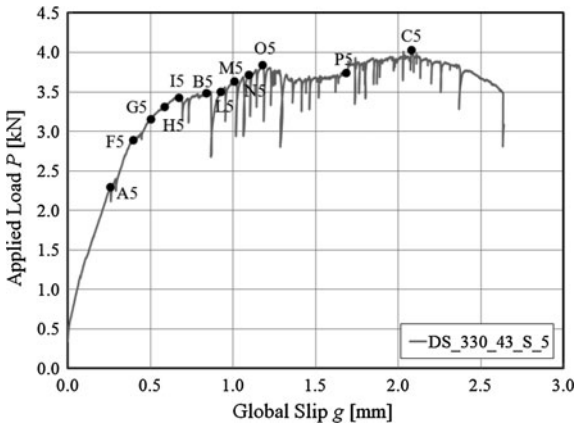

Fig. 9.13 Load response of specimen DS_330_43_S_5

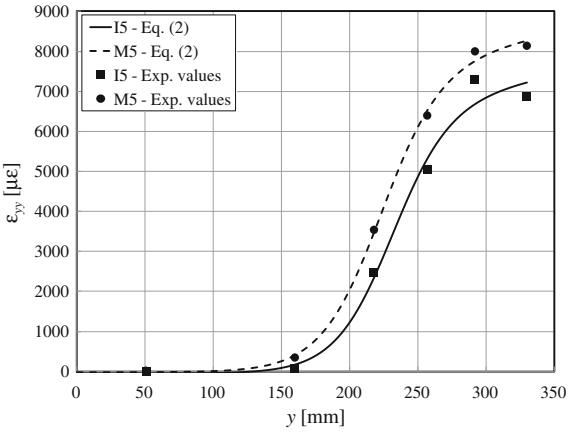

Fig. 9.14 Strain profiles and fitting curves corresponding to points I5 and M5 in the load response of DS_330_43_S_5 (Fig. 9.5)

$$\varepsilon_{yy} = \varepsilon_0 + \frac{\alpha + ky}{1 + e^{-\frac{y-y_0}{\beta}}} \tag{9.2}$$

where ε_0, α, β, and y_0 are determined using nonlinear regression analysis of the strains, whereas k is a coefficient that takes into account the presence of friction (D'Antino et al. 2014).

The strain profiles and the corresponding fitting curves based on Eq. (9.2) are shown in Fig. 9.14. The curves correspond to points I5 and M5 in the load response (see Fig. 9.13). The points were chosen in the region of the load response where the debonding initiated and friction between fibers and matrix is not present yet.

The fitting curves can potentially be used to obtain the effective bond length and the cohesive material law τ_{zy}-s, which relates the interfacial shear stress and the relative slip between the fibres and the matrix at any point along the bonded length. The shear stress can be determined from the gradient of the deformation (Subramaniam et al. 2007) while the slip can be determined by integration of ε_{yy}. The strain analysis carried out on the specimens equipped with strain gauges showed that an effective bond length, i.e. the minimum length needed to fully establish the stress-transfer mechanism (Subramaniam et al. 2011), exists. Provided that the friction between fibres and matrix and between fibre filaments is clearly identified, the strain profiles corresponding to the debonding load were analysed providing a value of the effective bond length l_{eff} of approximately 260 mm.

Strain gauges were also applied on the longitudinal fiber bundles of PBO FRCM-concrete joints where the external layer of matrix was omitted. Results were used to investigate the role of the internal and external matrix layer in the fiber-matrix stress-transfer mechanism (Carloni et al. 2014).

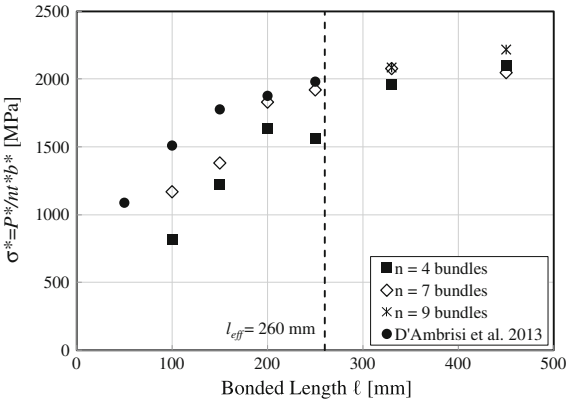

Fig. 9.15 Variation of the ultimate stress σ^* as a function of the bonded length ℓ

Effect of the Bonded Length

Figure 9.15 shows the average of the ultimate stress σ^* for each bonded width tested as a function of the bonded length ℓ for the tests herein presented. Three different bonded widths, namely 34 mm (n = 4), 60 mm (n = 7), and 80 mm (n = 9) are considered. The results of the double-lap shear tests published by D'Ambrisi et al. (2012, 2013b, c) are included for comparison in terms of the average of the ultimate stress σ^* for each bonded width. The results of Fig. 9.15 show that the ultimate stress σ^* increases as the bonded length ℓ increases up to a value equal to 450 mm. However, the ultimate stress appears to increase linearly when the bonded length is greater than 250 mm, confirming the existence of the effective bond length l_{eff}. The increase of the applied load when $\ell > l_{eff}$ is due to the friction between fibres and matrix and between fibre filaments.

Final Remarks on the Bond Behaviour for PBO-FRCM Composites

The results of single-lap direct-shear tests conducted on PBO FRCM-concrete indicate that the failure is characterized by debonding of the fibre within the embedding matrix. After the onset of debonding, the applied load is due both to the residual bond and the friction between matrix and fibres and between fibre filaments. The analysis of the peak stress for specimens with the same bonded length but different bonded width showed that, although a width effect within the single bundle can be recognized, a global width effect does not exist among multiple bundles and therefore for the entire width of the composite. Finally, the strain profiles along the bonded length in the load direction allowed for determining the value of the effective bond length.

Flexural Strengthening

This section provides an overview on the use of FRCM materials for flexural strengthening of RC structures. Experimental works are presented and discussed.

Introduction

The mechanical effectiveness of FRCM materials is strongly influenced by the bond between single fibers and matrix (Badanoiu and Holmgren 2003; Banholzer 2004; Banholzer et al. 2006; Hartig et al. 2008; Häußler-Combe and Hartig 2007; Hegger et al. 2006; Zastrau et al. 2008), which in turn is related to the matrix capacity of wetting single filaments (Badanoiu and Holmgren 2003; Banholzer 2004; Banholzer et al. 2006; Hartig et al. 2008; Häußler-Combe and Hartig 2007; Hegger et al. 2006; Zastrau et al. 2008), the bond between external fibers, directly in contact with the matrix, and internal fibers (Badanoiu and Holmgren 2003; Hartig et al. 2008; Häußler-Combe and Hartig 2007), the contribution of joints between longitudinal and transverse fibers (Soranakom and Mobasher 2009; Peled et al. 2008), and the cracking of the cement based matrix (Curbach et al. 2006; Ortlepp et al. 2004, 2006). Moreover, the matrix moderate capacity to penetrate into the free spaces among the fibers and the poor shear transfer among the single filaments can cause non uniformity of tensile stress in fibers of a roving and consequent fibers telescopic failure (Banholzer 2004; Banholzer et al. 2006; Hartig et al. 2008; Häußler-Combe and Hartig 2007; Hegger et al. 2006; Zastrau et al. 2008). In addition to these peculiarities, which are related to the characteristics of the FRCM system itself, in the case of FRCM materials used for the external strengthening of RC elements the strengthening effectiveness is also affected by bond between the cement-based matrix and the concrete substrate (Curbach et al. 2006; Ortlepp et al. 2004, 2006) and by the strength of the RC concrete substrate (Brückner et al. 2006; Curbach et al. 2006; Ortlepp et al. 2004, 2006). All these phenomena depend on the type, the surface treatment, and the geometrical arrangement of fibres, on the composition and grain fineness of the matrix, on the quality and the surface treatment of the concrete substrate. The shape of the fabric is of great importance (Curbach et al. 2006; Ortlepp et al. 2004, 2006) as the embedding of the rovings is ensured by the free spaces present in between the bundles because of the moderate cement based matrix capacity to impregnate single fibres due to its granularity. For this reason the surface of the matrix/roving interface should be maximized, e.g. by reducing the rovings dimension and simultaneously increasing the number of rovings, (Badanoiu and Holmgren 2003). Moreover, the presence of the fabric itself reduces the capacity of the matrix to transfer shear and tensile stresses through the thickness of the composite due to the surface reduction (Ortlepp et al. 2004, 2006).

Literature Review

Experimental and theoretical research works show that FRCM materials can be used effectively for the flexural strengthening of RC structures. Nevertheless, the comparison of results published by different researchers is difficult because of the differences in materials considered and test methods employed. FRCM systems comprised of different types of fibers, namely carbon, PBO, AR glass, steel, and basalt fibers, and different matrices have been considered by researchers for flexural strengthening applications of RC beams and slabs. In particular, carbon fibers were considered by Hashemi and Al-Mahaidi (2012a, b), Wiberg (2003), Pareek et al. (2007), Triantafillou (2010) and Täljsten and Blanksvärd (2007), PBO fibers were considered by Ombres (2009, 2011, 2012), and Bisby et al. (2009), basalt fibers were considered by Elsanadedy et al. (2013), and AR glass fibers were considered by Brückner et al. (2006). A comparison of FRCM systems with different types of fibers are reported in the works of Weiland et al. (2006) (AR glass vs. carbon), D'Ambrisi and Focacci (2011) (PBO vs. carbon) and Pellegrino and D'Antino (2013) (carbon vs. steel). In almost all of the aforementioned papers (Täljsten and Blanksvärd 2007; Pareek et al. 2007; Hashemi and Al-Mahaidi 2012a, b; Ombres et al. 2009; Bisby et al. 2009; Elsanadedy et al. 2013; D'Ambrisi and Focacci 2011; Pellegrino and D'Antino 2013; Triantafillou 2010) the flexural behavior of FRCM strengthened is compared with similar beams strengthened with FRP composites. The comparison indicated a similar strengthening effectiveness for FRCM and FRP composites, although in the most cases the FRP composites appear to be more effective than the FRCM composites when the same fibre cross section is considered. This fact is due to the better fibre impregnation by the epoxy resin, when compared to the cement-based mortar, which induces a uniform tensile stress among the fibres of the bundle.

FRCM materials have been used in several strengthening applications. Some applications are described in ACI (2013); the design criteria adopted for the FRCM-strengthening of a railway bridge are described in D'Ambrisi et al. (2013a, 2015).

Mechanical Effectiveness

The effectiveness of FRCM composites for flexural strengthening of RC beams is usually evaluated performing four points bending tests of unstrengthened and FRCM-strengthened RC beams (Fig. 9.16). Load deflection curves of unstrengthened and FRCM strengthened beams are compared in terms of maximum load and stiffness.

Referring to Fig. 9.16, experimental results available in the technical literature are relative to beams with ratio H/B ranging between 0.4 and 1.8 (prestressed beams and slabs are excluded) and ratio L_1/L ranging between 0.3 and 0.42. A very wide range can be observed in the ratio $\rho_f = A_f/A_c$ where A_f is the fiber cross-sectional area and A_c is the gross concrete cross-sectional area: this parameter ranged

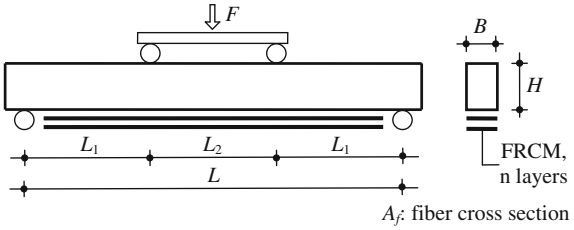

Fig. 9.16 Typical test setup for FRCM strengthened beams

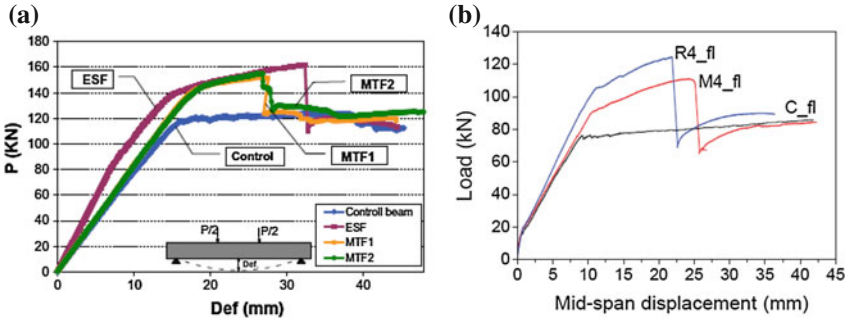

B = 140 mm, H = 260 mm, A_s = 339 mm^2, A_f = 28.2 mm^2, L = 2300 mm, L_1 = 700 mm. ESF: epoxy resin, MTF: cementitious mortar.

B = 150 mm, H = 250 mm, A_s = 226 mm^2, A_f = 22.6 mm^2, n = 4, L = 2000 mm, L_1 = 750 mm. R4_fl: epoxy resin, M4_fl: cementitious mortar.

Fig. 9.17 Experimental results of carbon FRCM strengthened RC beams obtained by **a** Hashemi and Al-Mahaidi (2012a, b) and **b** Triantafillou (2010); A_s is the cross-sectional area of steel rebar in tension

between 0.018 and 0.587 %. The number of fibre layers ranged between 1 and 10 but 2, 3, and 4 layers are the most frequently adopted numbers of layers.

The percentage flexural capacity increase depends on the specimens shape and the ratio between the area of steel and the area of fibers. The flexural capacity for carbon-FRCM composites increased from 10 to 100 %. It should be observed that the highest values correspond to the adoption of polymer-coated carbon fibre grid bonded to the concrete substrate with a cement based mortar (Täljsten and Blanksvärd 2007; Pareek et al. 2007). In the cases of dry fibres the flexural capacity increase typically ranged between 15 and 45 % with the application of 1–4 layers of fabric (Fig. 9.17).

In the case of PBO fibres the flexural capacity increase ranged between 15 and 150 %; typical values are around 20–50 % with the adoption of 1–4 layers of fabric (Fig. 9.18). In the case of steel fibres an increase of 24 % was found by Pellegrino and D'Antino (2013) in their experimental work on precast prestressed beams (Fig. 9.19).

Finally, in the case of basalt fibres a flexural capacity increase between 40 and 100 % was found in the experimental work of Elsanadedy et al. (2013) with the adoption of 5–10 fabric layers (Fig. 9.20).

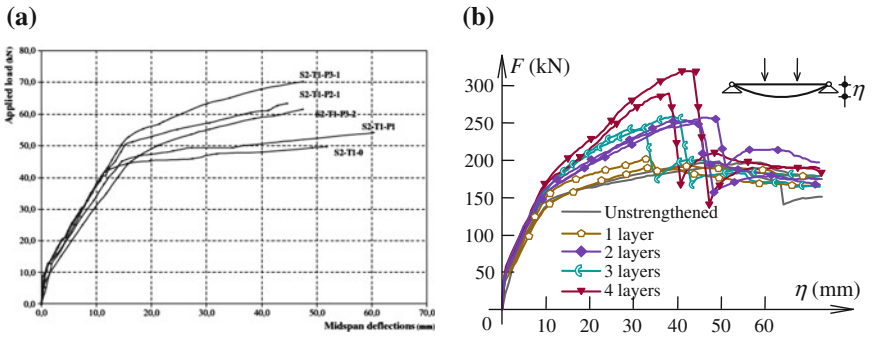

B = 150 mm, H = 240 mm, A_s = 157 mm^2, A_f = 6.75 mm^2/layer, L = 2700 mm, L_1 = 900 mm. S2-T1-P1: 1 layer; S2-T1-P2: 2 layers; S2-T1-P3: 3 layers.

B = 400 mm, H = 250 mm, A_s = 462 mm^2, A_f = 18.0 mm^2/layer, L = 2200 mm, L_1 = 750 mm.

Fig. 9.18 Experimental results of PBO FRCM strengthened RC beams obtained by **a** Ombres (2011) and **b** D'Ambrisi and Focacci (2011); A_s is the cross sectional area of steel rebar in tension

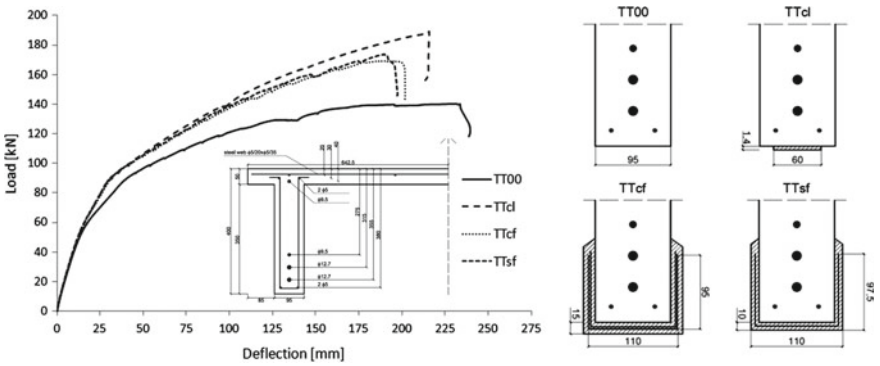

L = 10 m; L_1 = 3588 mm;

TT00: unstrengthened; TT cl: FRP strengthened with pultruded laminate (A_f = 168 mm$_2$, n = 1);

TTcf: carbon FRCM strengthened (A_f = 70.2 mm^2, n = 1);

TTsf: steel FRCM strengthened (A_f = 134.2 mm^2, n = 1).

Fig. 9.19 Experimental results of prestressed concrete beams strengthened with carbon and steel FRCM composites (Pellegrino and D'Antino 2013)

Failure Modes

The majority of the FRCM strengthened beams tested by the aforementioned authors failed due to the loss of composite action related to the debonding of the strengthening material from the supporting concrete. In FRC-strengthened beams the debonding can occur: at the matrix-fibre interface, at the matrix-concrete interface, and within the concrete. Depending on the type of fibres and matrix,

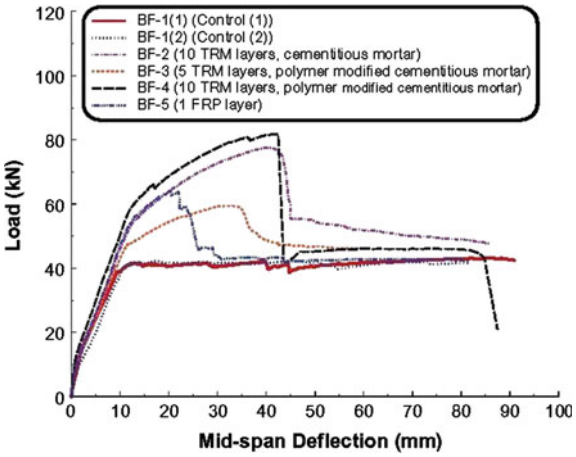

$B = 150$ mm, $H = 200$ mm, $A_s = 157$ mm^2,
$A_f = 9.6$ mm^2/layer, $L = 2000$ mm, $L_1 = 800$ mm

Fig. 9.20 Experimental results RC beams strengthened with basalt FRCM (Elsanadedy et al. 2013)

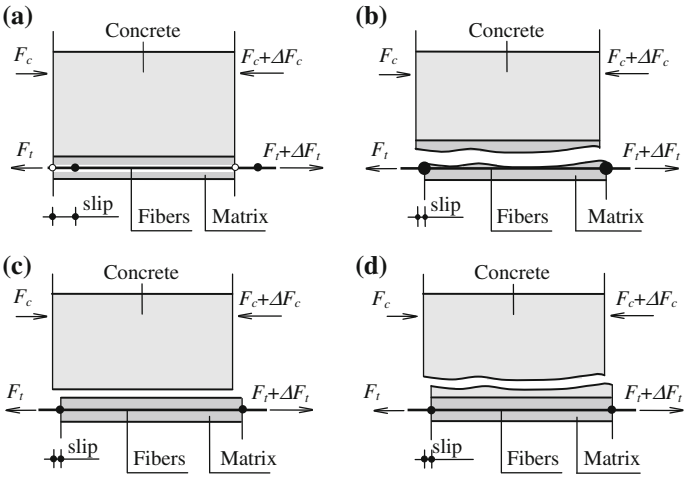

Fig. 9.21 Different possible debonding surfaces

different flexural debonding failure modes can be identified (D'Ambrisi and Focacci 2011), as schematically shown in Fig. 9.21.

Referring to Fig. 9.21, the failure modes reported in the literature are:

(a) Debonding of fibres from the matrix with high matrix-fibre slips (up to 1–2 mm) in the maximum bending moment region (Fig. 9.21a); this mode is typical for FRCM composites with dry carbon fibres embedded in a

cement-based matrix; although it has been also observed in a few cases with dry PBO fibres embedded in a cement-based matrix. During the matrix-fibres slip, the total force carried by fibres gradually decreases due to the gradual rupture of the fibres, eventually damaged by friction (Badanoiu and Holmgren 2003; Banholzer 2004; Banholzer et al. 2006; Häuβler-Combe and Hartig 2007; Zastrau et al. 2008). This type of debonding essentially involves the matrix-fibre and the fibre–fibre bond surfaces and it is not affected by the mechanical properties of the concrete substrate.

(b) Delamination with fracture surface within the matrix, preceded by considerable matrix-fibre slips (Fig. 9.21b); this failure mode has been observed in several beams strengthened with dry PBO fibres embedded in a cement-based matrix. It is essentially related by the matrix-fibre bond and the matrix tensile and shear strengths, while it is not affected by the mechanical properties of the supporting concrete.

(c) Deboning at the matrix-concrete interface, (Fig. 9.21c); this very brittle mode has been rarely observed and can generally be avoided with a proper preparation of the concrete surface before the application of the strengthening material. It involves the matrix-concrete bond.

(d) Debonding of the strengthening material with fracture surface within the concrete (a thin layer of concrete remains attached to the debonded strengthening material) (Fig. 9.21d). This very brittle mode has been rarely observed for FRCM strengthening systems. It is typical for FRP strengthened beams and essentially involves the mechanical properties of the supporting concrete.

The aforementioned debonding mechanisms are consistent with those described in (Ortlepp et al. 2004, 2006), D'Ambrisi et al. (2012, 2013a, b) and Carloni et al. (2013) for the case of simple or double shear tests.

Figure 9.22 shows the schematic shape of load-deflection diagrams of FRCM flexurally strengthened RC beams. After the steel bars yield (point A), the slope of the strengthened beams diagrams is related to the axial stiffness of the intrados strengthening material. In this phase small matrix-fibre slips occur locally at the

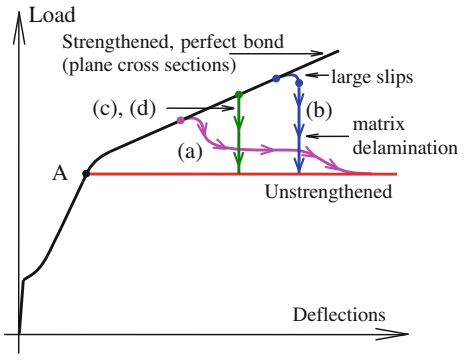

Fig. 9.22 Typical load-deflection curves of FRCM strengthened RC beams

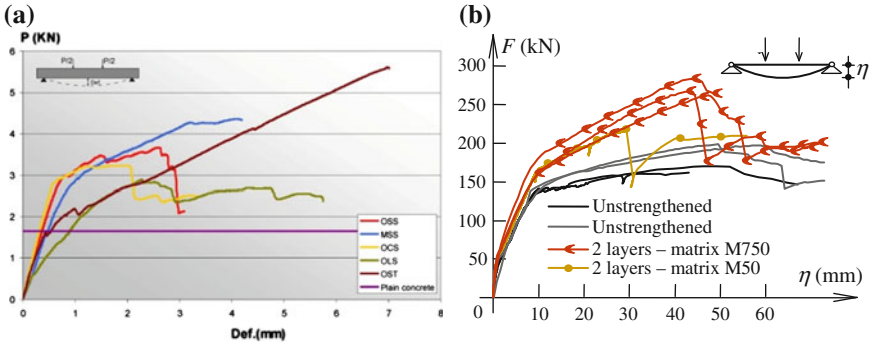

Carbon fibers. $A_f = 0$, $L = 750$ mm.
OCS: ordinary Portland cement - sheet.
OSS: silica fume incorporated – sheet.
OLS: polymer-modified mortar – sheet.
MSS: micro cement added to OC mortar – sheet.
OST: silica fume incorporated – textile.

PBO fibers. $B = 400$ mm, $H = 250$ mm,
$A_s = 462$ mm^2, $A_f = 36$ mm^2,
$L = 2200$ mm, $L_1 = 750$ mm.

Fig. 9.23 Effect of the matrix composition: experimental results of FRCM strengthened RC beams obtained by **a** Hashemi and Al-Mahaidi (2008) and **b** D'Ambrisi and Focacci (2011)

main flexural crack locations; nevertheless, the assumption of plane cross sections, including the strengthening material, allows for a good prediction of the experimental results. The post-yielding branch of the load-deflection diagram continues up to the loss of the strengthening action.

The loss of strengthening action can be sudden or more gradual, depending on the failure mode (a), (b), (c) or (d) (Fig. 9.21), corresponding to the schematic descending branches (a), (b), (c) or (d) of the load-deflection diagrams reported in Fig. 9.22.

The analytical prevision of the failure load requires the preliminary determination of the expected debonding failure mode among the four described above. This is not a simple task because it requires the determination of the hierarchy among the strengths related to the different bond failure surfaces. The hierarchy, in turn, depends on the type of fibres, type of matrix, fibres arrangement in the fabric, mechanical properties of matrix, and supporting concrete. Moreover, the strength hierarchy could also depend on the adopted number of fabric layers.

The important role played by the matrix-fibre bond induced several researchers (Hashemi and Al-Mahaidi 2008; Täljsten and Blanksvärd 2007; Elsanadedy et al. 2013; D'Ambrisi and Focacci 2011) to test different matrix compositions (Fig. 9.23). Figure 9.20 shows the results published by Elsanadedy et al. 2013 regarding a comparison between the performances of a cementitious mortar and a polymer modified cementitious mortar. These results confirm that, for a given fibre fabric, the strengthening effect drastically change with the adoption of different cement-based matrices.

The effect of end mechanical anchors applied to the flexural strengthening FRCM material was experimentally investigated by Hashemi and Al-Mahaidi

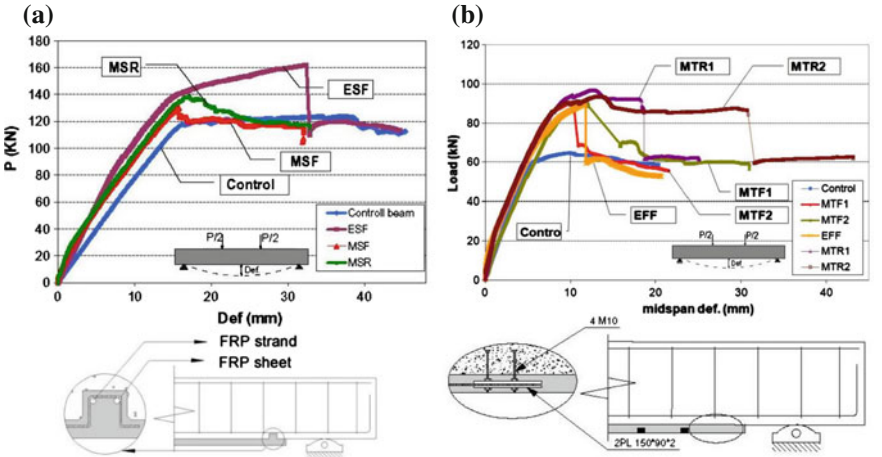

Carbon fibers. $B = 140$ mm, $H = 260$ mm, $A_s = 339$ mm^2, $A_f = 28.2$ mm^2, $n = 2$; $L = 2300$ mm, $L_1 = 700$ mm.
ESF: epoxy resin, MTF: cementitious mortar without connectors, MSR: cementations mortar with end connectors.

Carbon fibers. $B = 120$ mm, $H = 180$ mm, $A_s = 226$ mm^2, $A_f = 30$ mm^2, $L = 1300$ mm, $L_1 = 550$ mm.
EFF: epoxy resin, MTF: cementitious mortar without connectors, MTR: cementations mortar with end connectors.

Fig. 9.24 Effect of the end anchorage of FRCM strengthening materials: results obtained by **a** Hashemi and Al-Mahaidi (2012a) and **b** Hashemi and Al-Mahaidi (2012b)

(2012a, b). Their results are sumarized in Fig. 9.24, where it can be observed that this type of devices can effectively increase the FRCM debonding load.

Design Considerations

As described in the previous section, in the case of FRCM external strengthening of RC elements the bond stress transfer is a very complex phenomenon depending on type, surface treatment, geometrical arrangement of fibres, composition and grain fineness of the matrix, and on quality and surface treatment of the concrete. Despite this complexity, all the proposed design approaches (ACI 2013; Wiberg 2003; Curbach et al. 2006; Brückner et al. 2006; Ombres et al. 2009; Ombres 2011) are based on the assumption (Bernoulli) that cross sections remain plane during the deformation up to the flexural capacity (Fig. 9.25). The presence of the FRCM layer(s) is accounted for by introducing an additional term to the equations usually employed for un-strengthened RC elements. In a real application the FRCM material is applied when a preexisting tensile strain ε_0 exists (Fig. 9.25) in the concrete surface where the strengthening material is applied on, due to the dead loads. This approach requires the definition of the maximum tensile strain ε_{fe} attained by the fibres, called effective strain. Since the experimental works show that the failure of FRCM strengthened

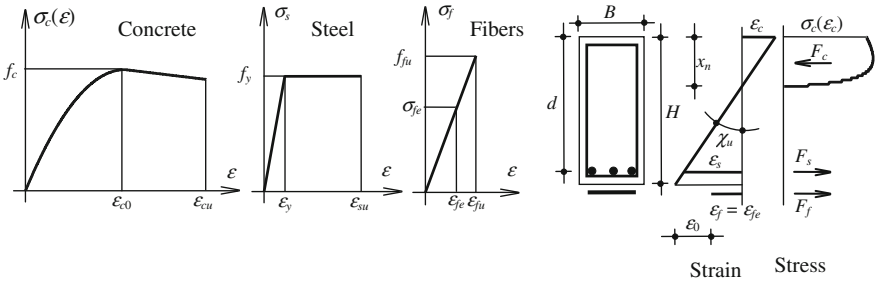

Fig. 9.25 Bernoulli assumption for an FRCM flexural strengthened RC cross section

beams is caused by the debonding (Fig. 9.21), the effective strain has to account for the loss of bond.

Following the guidelines ACI (2013), the effective strain is experimentally evaluated according to ICC (2013). Assuming that the member failure is reached when the effective tensile strain ε_{fe} in the FRCM reinforcement is attained and that the steel is yielded at failure, the flexural bending capacity is

$$M_R = B \cdot \int_0^{x_n} \sigma_c(\chi_u \cdot \xi) \cdot \xi \, d\xi + A_s \cdot f_{yd} \cdot (d - x_n) + A_f E_f \cdot \varepsilon_{fe} \cdot (H - x_n) \tag{9.3}$$

where $\sigma_c(\varepsilon)$ is the concrete compressive constitutive law, A_s is the cross-sectional area of the steel longitudinal reinforcement, A_f is the fibre cross-sectional area, E_f is the fibre elastic modulus. χ_u is the curvature at failure obtained as:

$$\chi_u = \frac{\varepsilon_{fe} + \varepsilon_0}{H - x_n} \tag{9.4}$$

The depth of neutral axis x_n is given by the equation

$$B \cdot \int_0^{x_n} \sigma_c(\chi_u \cdot \xi) \cdot d\xi = A_s \cdot f_y + A_f E_f \cdot \varepsilon_{fe} \tag{9.5}$$

In Eq. (9.4) ε_0 is the tensile strain of the concrete surface where the FRCM material is applied at the time of the FRCM application; the remaining symbols adopted in Eqs. (9.1)–(9.5) are defined in Fig. 9.25. In the most cases the flexural capacity can be approximated by

$$M_R = 0.9 \cdot A_s \cdot f_y \cdot d + 0.9 \cdot H \cdot A_f E_f \cdot \varepsilon_{fe} \tag{9.6}$$

The application of this approach requires only the definition of the effective strain of the fibres, which represents a strain limit globally accounting for the loss of bond. Similar approaches are suggested in CNR (2004), FIB (2001) and ACI (2008) for the case of flexural strengthening of RC structures with FRP composites. An important difference between the cases of FRP and FRCM materials is related to the type of debonding failure. In the case of flexural strengthening with FRP composites, the debonding usually occurs within the concrete. Therefore the effective strain ε_{fe} strongly depends on the concrete mechanical properties. In the case of flexural strengthening with FRCM composites debonding can occur at different bond surfaces, depending on the fibre type and arrangement, the type of matrix, and the mechanical properties of the concrete substrate. Therefore, the effective strain has to be evaluated for the particular FRCM material adopted. Since the most frequently observed failure modes are cases (a) and (b) represented in Fig. 9.21, the debonding strain should depend on the matrix-fiber interface properties and on the matrix mechanical properties rather than on the concrete properties, at least for the concrete substrates considered in the available literature.

Some of the cited experimental works (Hashemi and Al-Mahaidi 2012a, b; Pareek et al. 2007; Pellegrino and D'Antino 2013; Ombres 2011; Elsanadedy et al. 2013) involved the direct measure of the fibres strain during the beams flexural tests. In other cases this strain has been evaluated by means of finite element (Hashemi and Al-Mahaidi 2012a, b; Elsanadedy et al. 2013) or analytical (D'Ambrisi and Focacci 2011) investigations. The strain measured at the beams failure are summarized in Fig. 9.26, versus the equivalent fibres thickness adopted in the FRCM materials; only the results of those specimens that failed due to debonding of the strengthening material are included in Fig. 9.26.

In order to include also an estimate of the maximum fibres strain reached during the experimental work where a direct strain measure is not included, a simple estimation is performed applying the equation

$$\varepsilon_{fe} = \frac{\Delta M_R}{0.9 \cdot H \cdot A_f E_f} \tag{9.7}$$

where ΔM_R is the FRCM contribution to the failure bending moment, evaluated as

$$\Delta M_R = \frac{\Delta F_R}{2} \cdot L_1 \tag{9.8}$$

ΔF_R is evaluated as shown in Fig. 9.27. It should be observed that Eq. (9.7) gives a rough estimate of the maximum fibres strain because it considers the assumptions: (i) the internal moment arm at failure is $0.9H$ and it does not depend on the geometrical parameters of the cross section and on the mechanical properties of the materials; (ii) the contribution of the steel reinforcement to the flexural capacity is

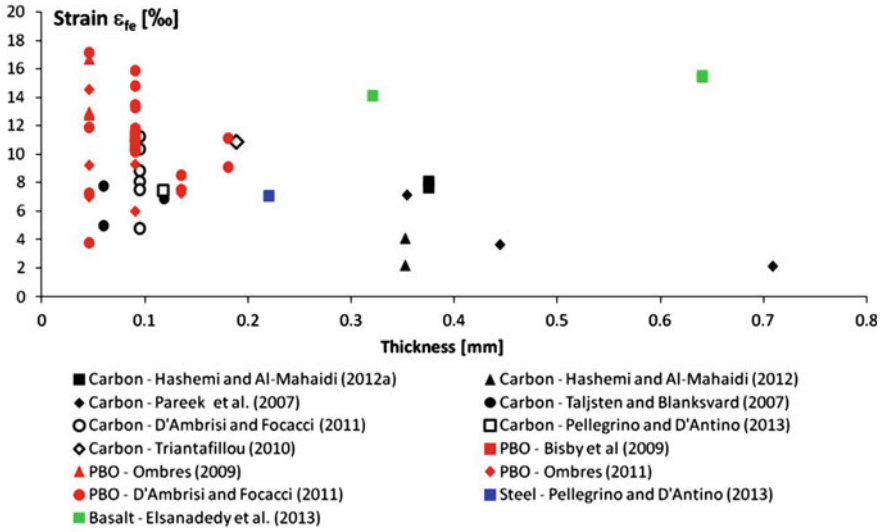

Fig. 9.26 Maximum fibres strain reached during the flexural tests of FRCM strengthened RC beams

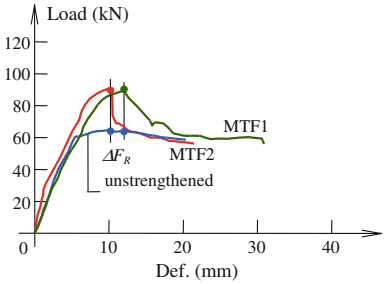

Fig. 9.27 Evaluation of ε_{fe} based on the experimental results of Hashemi and Al-Mahaidi (2012b)

the bending moment acting on the companion unstrengthened specimens at the same deflection. Nevertheless this approach allows for simply estimating the maximum fibres strain reached during the experimental tests. Moreover this estimated strain value has to be regarded as an average value on the fibre cross section; the phenomenon of the so-called telescopic failure, i.e. the successive fibre failure layer by layer from the outer to the inner fibres, (Badanoiu and Holmgren 2003; Banholzer et al. 2006; Häußler-Combe and Hartig 2007; Hegger et al. 2006; Zastrau et al. 2008) is not considered. However, the strain value is meaningful under the assumption that the debonding phenomenon is only related to the fibre

local strain value. The experimental results reported in papers where a direct measure of ε_{fe} is performed were used to compare the measured and the analytically determined values of ε_{fe}. On average a difference of 17 % was found. As an example, Fig. 9.27 shows the determination of ε_{fe} based on the results described in Hashemi and Al-Mahaidi (2012a). In this case for the specimen MTF1 it results

$$\Delta F_R = 26.95\,\text{kN} \tag{9.9a}$$

$$\Delta M_R = \frac{\Delta F_R}{2} \cdot L_1 = 7.41\,\text{kN} \tag{9.9b}$$

Consequently

$$\varepsilon_{fe} = \frac{\Delta M_R}{0.9 \cdot H \cdot A_f E_f} = 7.62\,‰ \tag{9.10}$$

where $H = 180$ mm is the cross-section height, and $E_f = 200$ GPa and $A_f = 30$ mm^2 are the elastic modulus and cross section of the fibres, respectively. Similarly, considering the specimen MTF2 the calculated value is $\varepsilon_{fe} = 7.14$. The measured value reported by the authors of ε_{fe} is 7.65 ‰ for the specimens MTF.

The results represented in Fig. 9.26 are quite scattered both in the case of carbon (black symbols) and in the case of PBO (red symbols) fibers. Moreover, a clear dependence of the strain ε_{fe} on the fibres thickness cannot be observed. In the case of carbon fibre the average value of ε_{fe} reported in Fig. 9.26 is 7.00 ‰ with a standard deviation of 2.7 ‰ (coefficient of variation 0.37), while in the case of PBO fibre the average value of ε_{fe} reported in Fig. 9.26 is 10.85 ‰ with a standard deviation of 3.24 ‰ (coefficient of variation 0.30). In the cases of basalt and steel fibres a smaller number of experimental results is currently available. The average ε_{fe} for the basalt fibre is 15.05 ‰ while the only available value for the steel fibres is 7.1 ‰. Figure 9.28 shows the average fibres tensile stress at debonding, obtained multiplying the strains of Fig. 9.26 by the elastic modulus of the fibres. In this case the PBO fibres seems to be more effective due to the fibres elastic modulus (270 GPa), which is higher than the carbon (200–240 GPa), the steel (205 GPa), and the basalt (32 GPa) elastic moduli of the fibres.

The experimental results considered show that the debonding strain covers a wide range depending on the specific FRCM material (type of fibres, type of matrix, fibres/matrix coupling, and arrangement of fibres). It is therefore necessary that the manufacturer of the strengthening material furnishes the proper parameters for the evaluation of the debonding strain. Moreover further research is needed to assess mechanical models able to estabilish the correct bond strength hierarchy among the bond strengths related to the different possible debonding surfaces.

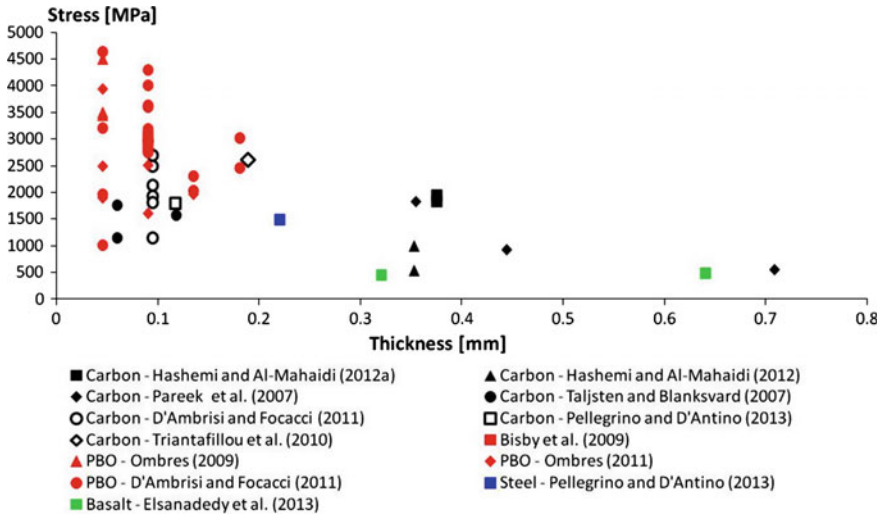

Fig. 9.28 Maximum fibres stress reached during the flexural tests of FRCM strengthened RC beams

Confinement

Confinement is generally applied to members in compression to enhance their axial load-carrying capacity, or to increase the deformation capacity of members subjected to seismic loading. Fibre-reinforced cementitious matrix composites, similarly to FRP, have an elastic behaviour and therefore exert an increasing confining action up to failure. This results in: (a) increasing concrete compressive strength and ultimate strain and (b) increasing the deformation capacity (ductility) of columns under seismic loading.

Jacketing of RC columns in existing structures is an increasingly attractive retrofit option. Among all jacketing techniques, the use of FRP has gained increasing popularity, due to the favourable properties possessed by these materials. However, certain problems associated with epoxy resins are still to be addressed. A solution of great potential, involving the combination of textiles with cement-based mortars for concrete confinement has been explored in very recent studies. TRM jackets have been investigated experimentally for confinement of plain or reinforced concrete and as a means of confining poorly detailed RC columns with limited deformation capacity under seismic loads. Comparison with FRP-retrofitted counterpart specimens allows for the evaluation of the effectiveness of TRM versus FRP jackets.

Behaviour of TRM-Confined Concrete in Axial Compression

Triantafillou et al. (2006) investigated experimentally for the first time the confinement effectiveness of various TRM jacketing schemes for plain concrete. That investigation was carried out on: (1) cylindrical specimens with a diameter of 150 mm and a height of 300 mm; (2) short column-type specimens with a rectangular cross section of 250 × 250 mm and a height of 700 mm. The four corners of all rectangular prisms were rounded at a radius equal to 15 mm. All specimens were unreinforced, as the jacket-reinforcement interactions were outside the scope of that study. Based on the response of confined cylinders, it was concluded that: (1) textile-mortar confining jackets provide substantial gain in compressive strength and deformability. This gain is higher as the number of confining layers increases and depends on the tensile strength of the mortar, which determines whether failure of the jacket will occur due to fibre fracture or debonding; (2) compared with their resin-impregnated counterparts, mortar-impregnated textiles may result in reduced effectiveness, in the order of approximately 80 % for strength and 50 % for ultimate strain, for the specific mortar used in that study; and (3) failure of mortar-impregnated textile jackets is less abrupt compared with that of their resin-impregnated counterparts, due to the slowly progressing fracture of individual fibre bundles. From the response of rectangular columns, it was concluded that mortar-impregnated textile jackets are quite effective in confining columns of rectangular cross sections for strength and axial deformability. In comparison with their epoxy-based counterparts, mortar-impregnated textile jackets provide approximately the same effectiveness in terms of strength and a slightly inferior one in terms of ultimate strain.

Bournas et al. (2007) went one step further by investigating experimentally the use of TRM jackets as a means of confining reinforced concrete. The experimental program aimed to compare the effectiveness of TRM versus FRP jackets as a measure of confining RC members. To examine this, 15 short RC prisms were tested under concentric compression. Specimens had a 200 mm ξ 200 mm cross section and a height of 380 mm. The prisms were divided in three series, with five specimens each. The first series comprised specimens with no internal steel reinforcement (Series U). The prisms in the second and third series were reinforced with four longitudinal 12 mm diameter bars placed at the corners of the cross section and with 8 mm diameter stirrups (Fig. 9.29).

The main interest in that study as far as the steel reinforcement is concerned was the spacing of stirrups. Hence, the second series comprised stirrups at a relatively large spacing of 200 mm (Series s200), to emulate old detailing practices. And in the last series (s100) the spacing was much smaller, equal to 100 mm, to represent current detailing practices. Each of the three series was comprised five different specimens: the control specimen (without wrapping), specimens wrapped with two or three layers of FRP and specimens wrapped with four or six layers of TRM. Note that the layers in the TRM-jacketed prisms were twice as many compared with their FRP counterparts, resulting in two "equivalent" confining systems that is with equal

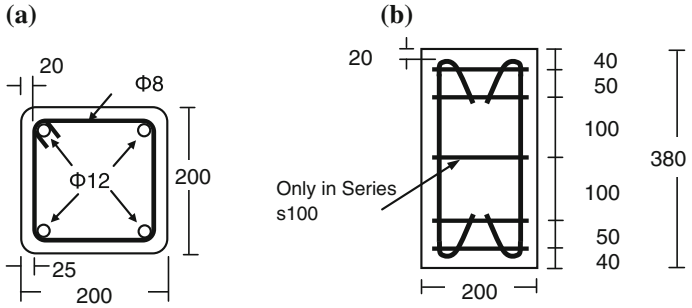

Fig. 9.29 **a** Cross section of prisms. **b** Configuration of reinforcement. (Dimensions in mm). (Bournas et al. 2007)

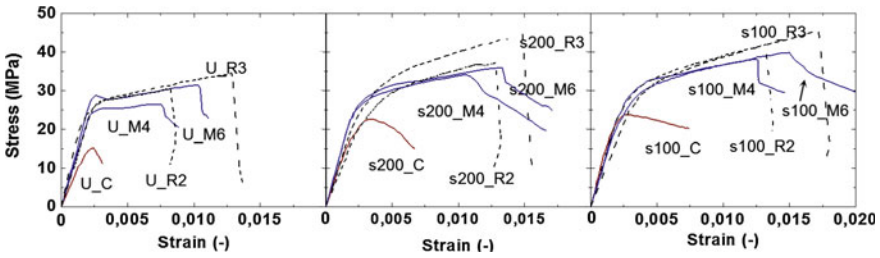

Fig. 9.30 Stress–strain curves for specimens: **a** without reinforcement; **b** with stirrups at 200 mm; **c** with stirrups at 100 mm (Bournas et al. 2007)

stiffness and strength in the circumferential direction. The notation of specimens is X_YN, where X refers to the internal steel reinforcement (U, s200, s100), Y denotes the type of jacket (C for the unjacketed—control—prisms, R for resin-based jackets and M for mortar-based jackets) and N denotes the number of layers.

The stress–strain plots recorded for all specimens are given in Fig. 9.30. All plots of the confined specimens are characterized by an ascending branch, followed by a second one, close to linear, that drops at a point where the jacket fractured due to hoop stresses (Fig. 9.31a); it is this point where peak stress and ultimate strain is defined, except for the control (unjacketed) specimens, where ultimate strain is defined conventionally at 15 % peak stress reduction. In some of the TRM-jacketed prisms (s200_M4, s100_M6) fracture of the fibres was accompanied by debonding at the end of the lap (Fig. 9.31b). In several occasions jacket rupture occurred simultaneously with bar buckling. Hence, failure of the jackets was due to stretching both by concrete dilation and by the outwards bending of the longitudinal bars in the middle of the specimens (Fig. 9.31c). Another important aspect of the response is that, contrary to FRP jackets, TRM jackets, did not fail abruptly since TRM jackets fracture initiates from a limited number of fibre bundles (when the

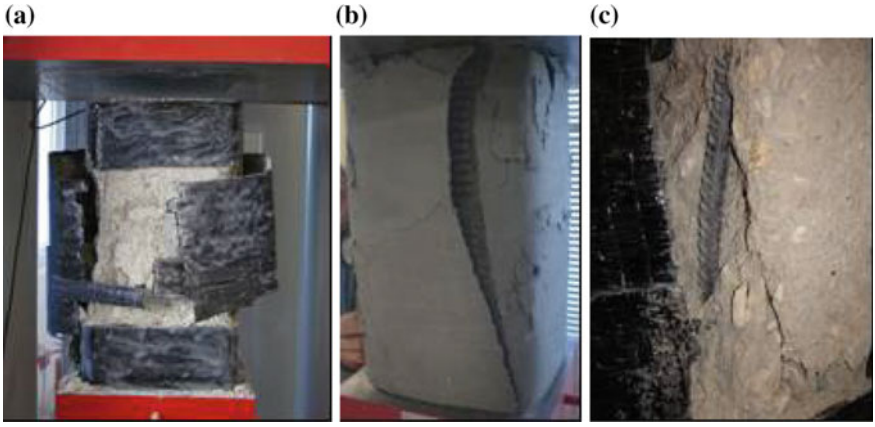

Fig. 9.31 **a** Fracture of jacket. **b** Debonding at the end of the lap. **c** Buckling of bar at corner (Bournas et al. 2007)

hoop stresses reach their tensile capacity) and then propagates rather slowly in the neighbouring bundles, resulting in a more ductile failure mechanism compared to FRP.

Overall, the concentric compression tests performed by Bournas et al. (2007) on RC prisms show that TRM confining jackets provide substantial gain in compressive strength and ultimate strain; this gain increases with the volumetric ratio of the TRM wrap. Compared with equal stiffness and strength FRP jackets, the TRM jackets used in Bournas et al. (2007) are slightly less effective in terms of increasing strength and deformation capacity by about 10 %. This reduction in effectiveness did not seem to depend on the volumetric ratio of the embedded stirrup reinforcement.

Behaviour of TRM-Confined Columns Under Cyclic Loading

More recently Bournas et al. (2009) investigated experimentally the use of TRM jackets as a means of confining poorly detailed old-type RC columns, which suffer from limited deformation capacity under seismic loads due to either buckling of the longitudinal bars or bond failure at lap splice regions. A total of 10 large-scale old-type RC columns were tested under cyclic uniaxial flexure with constant axial load (Fig. 9.32a). In Bournas et al. (2009) four specimens were constructed with continuous longitudinal reinforcement (Series L0). One specimen was tested without retrofitting, as control (L0_C), the second one was retrofitted with a double-layered CFRP jacket (specimen L0_R2), the third one was retrofitted with an equal (to its FRP counterpart) stiffness and strength carbon fibre TRM jacket comprising four layers (specimen L0_M4), and the last specimen was retrofitted

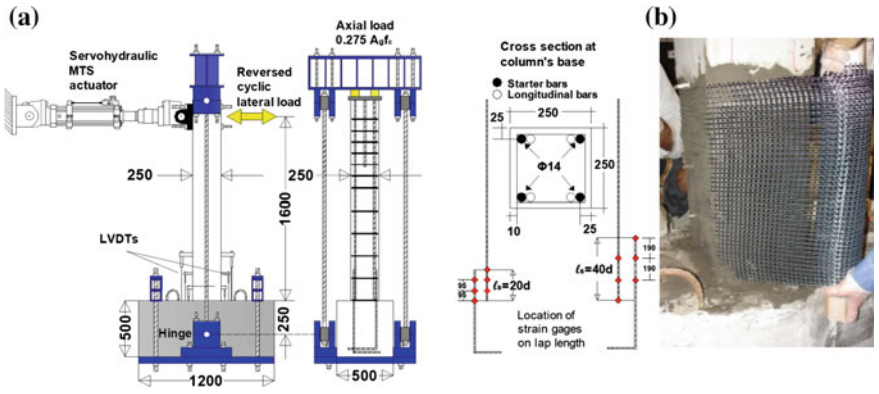

Fig. 9.32 **a** Schematic of test setup and cross section of the columns. **b** Application of a TRM jacket

with a lower stiffness and strength four-layered glass fibre TRM jacket (specimen L0_M4G), which represents a rehabilitation solution of lower cost in comparison with specimen L0_R2 and L0_M4.

The effectiveness of TRM versus FRP jackets, applied at the ends of old-type RC columns for specimens constructed with lap splicing of longitudinal reinforcement above the column base, was evaluated for two different lap lengths, which were selected equal to 20 and 40 bar diameters, as shown in Fig. 9.32a. In summary, the notation of specimens is LX_YN, where X defines the lap splice length above the column base (0 for continuous reinforcement, 20d for a lap splice length of 20 rebar diameters, 40d for a lap splice length of 40 rebar diameters), Y denotes the type of jacket (C for the unjacketed—control—columns, R for resin-based jackets, and M for mortar-based jackets) and N denotes the number of layers. For the specimen strengthened with a glass fibre TRM jacket the letter G was added after letter N. The jackets extended from the base of each column to a height of 430 mm except for the two columns with longer lap splices (L40d_R2 and L40d_M4) where the jackets were extended to a height of 600 mm. The overlapping length of the jacket was equal to 150 mm. Prior to jacketing, the four corners of the columns which received jacketing were rounded at a radius equal to 25 mm. A photograph of the application method of textile combined with mortar binder to provide jacketing in one of the specimens used in Bournas et al. (2009) is shown in Fig. 9.32b.

The response of the columns tested in Bournas et al. (2009) is given in Fig. 9.33 in the form of load-drift ratio loops. Key results are also presented in Table 9.2, which includes: (a) The peak resistance in the two directions of loading. (b) The drift ratio corresponding to peak resistance in the two directions of loading. (c) The drift ratio at conventional "failure" of the column, defined as reduction of peak resistance in a cycle below 80 % of the maximum recorded resistance in that direction of loading. (d) The observed failure mode.

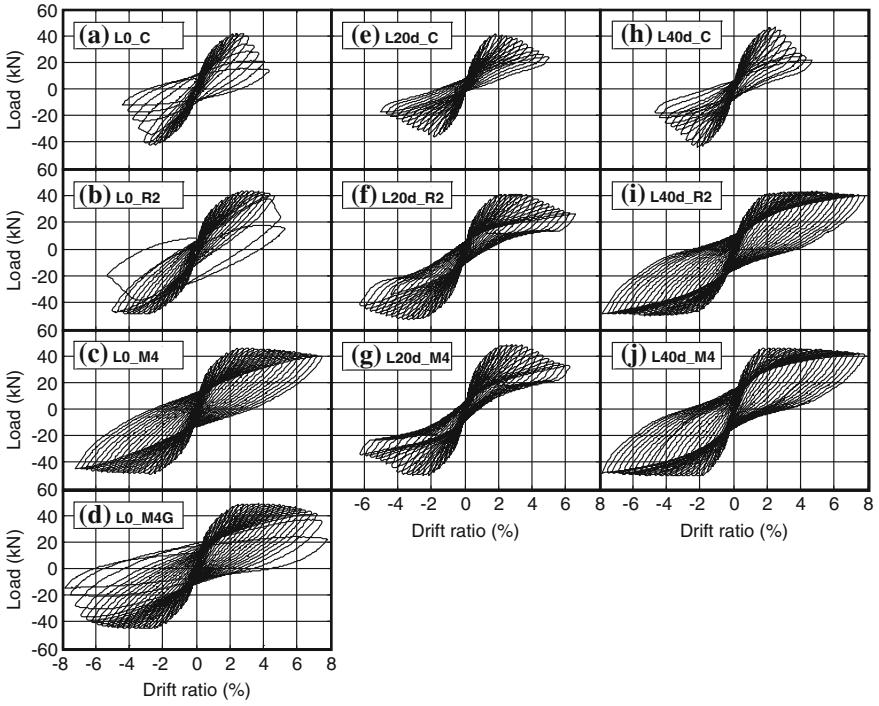

Fig. 9.33 Load versus drift ratio curves for all specimens tested in Bournas et al. (2009)

The failure mode of the unretrofitted specimen with continuous bars was controlled by bar buckling (Fig. 9.34a) with a sustained drift ratio at failure of 3.43 %.

The confinement provided by the FRP jacket to specimen L0_R2 restrained the outward bending of longitudinal bars inside the FRP jacket region, but bar buckling finally occurred above the FRP jacket (Fig. 9.34b) at a drift equal to 5.15 %. Contrary to specimen L0_R2, rebar buckling in columns L0_M4 and L0_M4G developed gradually inside the TRM-jacketed area, as the compressive force released from early buckled bars was carried by the surrounded confined concrete inside the jackets. This is possible to occur in this confining system, as TRM jackets are able to deform outwards without early fibre rupture, due to the low composite action between fibres and mortar, which allows for higher local deformations (e.g. slip of fibres within rovings). In specimen L0_M4 the carbon fibre TRM jacket remained intact until the test was terminated at drift ratio equal to 7.81 % (Fig. 9.34c), while in specimen L0_M4G fracture of the glass fibre TRM jacket (at a drift ratio equal to 7.2 %) led to failure (Fig. 9.34d).

The failure mode of the control specimens with lap splices was characterized by splitting cracks, developed along the splice length of lapped bars, for both unretrofitted specimens L20d_C and L40d_C, respectively. The drift ratio at failure sustained by unretrofitted columns L20d_C and L40d_C was 3.59 and 3.28 %,

Table 9.2 Summary of test results (Bournas et al. 2009)

Specimen notation	Peak force (kN)		Drift at peak force (%)		Drift at "failure" (%)		Failure mode
	Push	Pull	Push	Pull	Push	Pull	
L0_C	41.63	−42.48	2.5	2.5	3.43	3.43	Buckling of longitudinal bars
L0_R2	43.46	−48.70	2.8	3.1	5.0	−5.31	Buckling of longitudinal bars above FRP jacket
L0_M4	45.77	−49.19	2.8	2.8	>7.81	>7.81	Conventional failure was not reached
L0_M4G	48.82	−45.28	4.0	2.8	7.5	6.9	Fracture of the TRM jacket due to both rebars buckling and concrete dilation
L20d_C	41.50	−36.62	1.87	1.87	4.06	3.12	Splitting bond failure followed by spalling of the concrete cover
L20d_R2	41.26	−52.86	2.81	3.12	5.31	6.25	Splitting longitudinal cracking followed by pull out bond failure of lapped bars
L20d_M4	48.46	−49.80	3.12	2.18	5.0	5.0	Splitting longitudinal cracking followed by pull out bond failure of lapped bars
L40d_C	46.26	−43.82	2.5	2.18	3.43	3.12	Splitting bond failure followed by spalling of the concrete cover
L40d_R2	42.97	−49.93	4.68	5.0	>7.81	>7.81	Conventional failure was not reached
L40d_M4	45.90	−50.48	1.87	3.75	>7.81	>7.81	Conventional failure was not reached

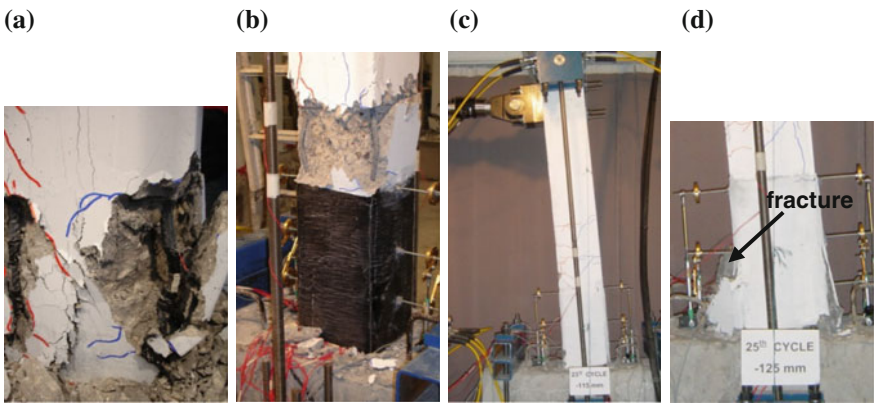

Fig. 9.34 **a** Disintegration of concrete and bar buckling. **b** Buckling of longitudinal bars above the FRP jacket. **c** Undamaged carbon TRM jacket at end of test. **d** Fracture of glass TRM jacket due to bar buckling

respectively. TRM and FRP jacketed columns, with either short or long lap length, responded far better than their unretrofitted counterparts. Confinement provided sufficient resistance against splitting cracks and lateral expansion of concrete. Specimens L20d_R2 and L20d_M4 (with short lap lengths) sustained reversed deformation cycles up to 6.3 % drift at failure. The mean strength increase for columns L20d_R2 and L20d_M4 was 20.3 and 25.6 %, respectively, in comparison with the control specimen (L20d_C), while the corresponding increase in deformation capacity was 64.7 and 38.8 %, respectively. Columns with longer lap splices (L40d_R2 and L40d_M4) behaved in an identical manner until the end of the test at a drift ratio of 7.81 % (maximum stroke of piston was reached), resulting in an increase of the member deformation capacity by a factor of more than 2.5. Peak resistance was practically the same as in the unretrofitted column (L40d_C).

The tests on columns with continuous longitudinal reinforcement (Series L0) show that TRM jackets are quite effective as a means of increasing the cyclic deformation capacity and the energy dissipation of old-type RC columns with poor detailing, by delaying bar buckling. Compared with equal stiffness and strength FRP, TRM jacketing has a higher effectiveness by about 50 %. From the tests on columns with lap-spliced longitudinal reinforcement (Series L20d and L40d), it may be concluded that TRM confining jackets provide substantial gain in lateral strength and deformation capacity of cyclically loaded reinforced concrete columns with lap splices at the base of the column. Compared with equal stiffness and strength FRP jackets, they are characterized by a slightly reduced effectiveness in terms of deformation capacity for columns with short lap splices and with the same effectiveness for columns with longer lap lengths. Detailed results on the bond strength of lap-spliced bars and bar buckling in TRM confined concrete are presented in Bournas et al. (2011a, b) and Bournas and Triantafillou (2011).

Deformation Capacity of TRM-Confined RC Members

The cyclic deformation capacity of RC columns, a key property in displacement-based design used in seismic rehabilitation applications, is typically expressed through the attained drift ratio of the members at failure. This important parameter for all specimens tested is compared in this section with predictions given by Eurocode 8 (EN 1998-3 2005). The drift ratio, which is defined as chord rotation capacity at ultimate in EN 1998-3 (2005), is given by the following empirical expression:

$$\theta_u = k0.016(0.3^{\nu})\left[\frac{\max(0.01,\omega')}{\max(0.01,\omega)}f_c\right]^{0.225}\left(\frac{L_V}{h}\right)^{0.35}25^{c}\left(1.25^{100\rho_d}\right) \qquad (9.11)$$

where f_c = compressive strength of concrete (MPa); ω and ω' = mechanical reinforcement ratio of tension and compression longitudinal reinforcement,

respectively; $v = N/bhf_c$ = normalized axial force (compression taken as positive); b = width of compression zone; h = cross section side parallel to the loading direction; $L_V = M/V$ = moment-to-shear ratio at the end section; $c = \alpha\rho_{sx}f_{yw}/f_c$; $\rho_{sx} = A_{sw}/bs_h$ = transverse steel ratio parallel to the direction x of loading; f_{yw} = yield stress of stirrups; s_h = spacing of stirrups; A_{sw} = area of transverse steel reinforcement parallel to the direction x within s_h; $k = 0.825$ for columns with deformed bars, without detailing for earthquake resistance; ρ_d = geometric ratio of diagonal reinforcement, if any; and α = effectiveness coefficient for confinement with stirrups.

If a column is retrofitted with an FRP or TRM jacket in the plastic hinge region, it is logical: (a) to take k equal to 1 instead of 0.825, as the lack of detailing for earthquake resistance has been compensated by the external confinement; and (b) to adopt the expression in Eq. (9.11) with c given by the sum of two terms: one to account for the contribution of stirrups and a second one to account for the contribution of the jacket, as follows (Bournas et al. 2007):

$$c = a\rho_{sx}\frac{f_{yw}}{f_c} + a_f\rho_{fx}\frac{f_{fe}}{f_c} \tag{9.12}$$

where $\rho_{fx} = 2nt_f/b$; n = number of layers of the fibre sheet or textile; t_f = thickness of one fibre sheet or textile layer; f_{fe} = effective stress of jacket at conventional failure of the column; and α_f = effectiveness coefficient for confinement with fibres (TRM or FRP jackets), equal to:

$$\alpha_f = \beta\left[1 - \frac{(b-2R)^2+(h-2R)^2}{3bh}\right] \tag{9.13}$$

where R = radius at corners of the cross section. The coefficient β in Eq. (9.13) accounts for the reduced or enhanced effectiveness of TRM versus FRP jackets in terms of ultimate strain. On the basis of concentric compression tests on reinforced concrete prisms presented in Triantafillou et al. (2006) and summarized above, this value is about 0.9. But if jacket failure has not been reached at conventional failure of the column, no reduction (nor enhancement) should be made and β should be taken equal to 1 (i.e. specimen L0_M4). It should be noted that in view of the relatively limited experimental database on TRM jacket failures, this value of β should be carefully selected. Other materials (e.g. different mortars) may result in different values for the effectiveness of TRM versus FRP. Therefore for such novel materials much more experimental work is needed to propose design values of β.

References

American Concrete Institute (ACI). (2008). Guide for the design and construction of externally bonded FRP systems for strengthening concrete structures. ACI 440.2R-08, Farmington Hills, MI.

American Concrete Institute (ACI). (2013). Guide to Design and Construction of Externally Bonded Fabric-Reinforced Cementitious Matrix (FRCM) Systems for Repair and Strengthening Concrete and Masonry Structures. ACI 549.4R-13, Farmington Hills, MI.

ASTM. (1996) Standard test method for tensile properties of polymer matrix composite materials. D3039/D3039 M, ASTM International, 6 pages.

ASTM. (2011a) Standard test method for compressive strength for cylindrical concrete specimens. C39/C39 M-12, ASTM International, 7 pages.

ASTM. (2011b) Standard test method for splitting tensile strength of cylindrical concrete specimens. C496/C496 M, ASTM International, 5 pages.

Badanoiu, A., & Holmgren, J. (2003). Cementitious composites reinforced with continuous carbon fibers for strengthening of concrete structures. *Cement & Concrete Composites, 25*, 387–394.

Banholzer, B. (2004). *Bond behaviour of a multi-filament yarn embedded in a cementitious matrix*. Ph.D. Thesis, RWTH Aachen University.

Banholzer, B., Brockmann, T., & Brameshuber, W. (2006). Material and bonding characteristics for dimensioning and modeling of textile reinforced concrete (TRC) elements. *Materials and Structures, 39*, 749–763.

Bisby, L. A., Roy, E. C., Ward, M., & Stratford, T. J. (2009). Fibre reinforced cementitious matrix systems for fire-safe flexural strengthening of concrete: Pilot testing at ambient temperature. In *Proceedings Advanced Composites in Construction, Edinburgh, UK*.

Bournas, D., Lontou, P., Papanicolaou, C. G., & Triantafillou, T. C. (2007). Textile-Reinforced Mortar (TRM) versus FRP Confinement in Reinforced Concrete Columns. *ACI Structural Journal, 104*(6), 740–748.

Bournas, D. A., & Triantafillou, T. C. (2011a). Bar Buckling in RC Columns Confined with Composite Materials. *Journal of Composites for Construction, 15*(3), 393–403.

Bournas, D. A., & Triantafillou, T. C. (2011b). Bond Strength of Lap Spliced Bars in Concrete Confined with Composite Materials. *Journal of Composites for Construction, 15*(2), 156–167.

Bournas, D. A., Triantafillou, T. C., Zygouris, K., & Stavropoulos, F. (2009). Textile-reinforced mortar (TRM) versus FRP jacketing in seismic retrofitting of RC columns with continuous or lap-spliced deformed bars. *Journal of Compososites for Construction, 13*(5), 360–371.

Brückner, A., Ortlepp, R., & Curbach, M. (2006). Textile reinforced concrete for strengthening in bending and shear. *Materials and Structures, 39*, 741–748.

Carloni, C., D'Antino, T., Sneed, L. H., & Pellegrino, C. (2014). Role of the matrix layers in the stress-transfer mechanism of FRCM composites bonded to a concrete substrate. *Journal of Engineering Mechanics, ASCE*. doi:10.1061/(ASCE)EM.1943-7889.0000883.

Carloni, C., Sneed, L. H., & D'Antino, T. (2013). Interfacial bond characteristics of fiber reinforced cementitious matrix for external strengthening of reinforced concrete members. In *Proceedings of the 8th international Conference on Fracture Mechanics of Concrete and Concrete Structures (FraMCoS-8), Toledo (Spain)* (pp. 129–137).

Carloni, C., & Subramaniam, K. V. (2012). Application of fracture mechanics to debonding of FRP from RC members. ACI SP-286: 10-1-10-14.

Carozzi, F. G., & Poggi, C. (2015). Mechanical properties and debonding strength of Fabric Reinforced Cementitious Matrix (FRCM) systems for masonry strengthening. *Composites: Part B*, *70*, 215–230.

Contamine, R., Si LArbi, A., & Hamelin, P. (2011). Contribution to direct tensile testing of textile reinforced concrete (TRC) composites, *Material Science and Engineering A, 528,* 8589–8598.

Curbach, M., Ortlepp, R., & Triantafillou, T. C. (2006). TRC for rehabilitation. In W. Brameshuber (Ed.), *Textile Reinforced Concrete* (pp. 221–236), RILEM Report 36.

D'Ambrisi, A., & Focacci, F. (2011). Flexural strengthening of RC beams with cement based composites. *Journal of Composites for Construction, 15*(2), 707–720.

D'Ambrisi, A., Feo, L., & Focacci, F. (2012). Bond-slip relations for PBO-FRCM materials externally bonded to concrete. *Compos Part B*, *43*(8), 2938–2949.

D'Ambrisi, L., Focacci, F., & Caporale, A. (2013a). Strengthening of masonry–unreinforced concrete railway bridges with PBO-FRCM materials. *Composite Structures*, *102*, 193–204.

D'Ambrisi, A., Feo, L., & Focacci, F. (2013b). Experimental analysis on bond between PBO-FRCM strengthening materials and concrete. *Composites—Part B, 44*(1), 524–532.

D'Ambrisi, A., Feo, L., & Focacci, F. (2013c). Experimental and analytical investigation on bond between carbon-FRCM materials and masonry. *Compos Part B*, *46*, 15–20.

D'Ambrisi, A., Focacci, F., Luciano, R., Alecci, V., & De Stefano, M. (2015). Carbon-FRCM materials for structural upgrade of masonry arch road bridges. *Compos Part B*, *75*, 355–366.

D'Antino, T., Carloni, C., Sneed, L. H., & Pellegrino, C. (2014). Matrix-fiber bond behavior in PBO FRCM composites: a fracture mechanics approach. *Engineering Fracture Mechanics, 117*, 94–111.

D'Antino, T., Carloni, C., Sneed, L. H., & Pellegrino, C. (2015). Fatigue and Post-fatigue Behavior of PBO FRCM-Concrete Joints. *International Journal of Fatigue*. doi:10.1016/j.ijfatigue.2015.06.008.

D'Antino, T., Sneed, L.H., Carloni, C., & Pellegrino, C. (2013). Bond behavior of the FRCM-concrete interface. In *Proceedings of 11th international symposium on fiber reinforced polymer reinforcement for concrete structures (FRPRCS-11), Guimaraes, Portugal*.

Elsanadedy, H. M., Almusallam, T. H., Alsayed, S. H., & Al-Salloum, Y. A. (2013). Flexural strengthening of RC beams using textile reinforced mortar—Experimental and numerical study. *Composite Structures, 97*, 40–55.

Féderation Internationale du Béton (FIB) (2001). Externally bonded FRP reinforcement for RC structures. Bulletin 14, Lausanne, Switzerland.

Hartig, J., Häußler-Combe, U., & Schicktanz, K. (2008). Influence of bond properties on the tensile behaviour of Textile Reinforced Concrete. *Cement & Concrete Composites, 30*, 898–906.

Hartig, F., Jesse, F., Schicktanz, K., & Häußler-Combe, U. (2012). Influence of experimental setups on the apparent uniaxial tensile load-bearing capacity of textile reinforced concrete specimens. *Materials and Structures, 45*, 433–446.

Hashemi, S., & Al-Mahaidi, R. (2008). Cement based bonding material for FRP strengthening of RC structures. In *Proceedings of 11th International Inorganic-Bonded Fiber Composites Conference (IIBC), Toledo, Spain*.

Hashemi, S., & Al-Mahaidi, R. (2012a). Experimental and finite element analysis of flexural behavior of FRP-strengthened RC beams using cement-based adhesives. *Construction and Building Materials, 26*, 268–273.

Hashemi, S., & Al-Mahaidi, R. (2012b). Investigation of flexural performance of RC beams strengthened with CFRP textile and cement based adhesives. In *Proceedings of the 3rd Asia-Pacific Conference on FRP in Structures (APFIS 2012)*, Hokkaido, Japan.

Häußler-Combe, U., & Hartig, J. (2007). Bond and failure mechanisms of textile reinforced concrete (TRC) under uniaxial tensile loading. *Cement and Concrete Composites, 29*, 297–289.

Hegger, J., Will, N., Bruckermann, O., & Voss, S. (2006). Load-bearing behavior and simulation of textile reinforced concrete. *Materials and Structures, 39*, 765–776.

ICC Evaluation Service. (2013). Acceptance Criteria for Masonry and Concrete Strengthening Using Fiber-reinforced Cementitious Matrix (FRCM) Composite Systems. AC434-2013.

Italian National Research Council (CNR). (2004). Guide for the design and construction of externally bonded FRP systems for strengthening existing structures. CNR-DT200/2004, Rome.

Jesse, F., Schicktanz, K., & Curbach, M. (2009). Obtaining Characteristic Material Strength of Textile Reinforced Concrete (TRC) from Laboratory Tests. In *Proceedings of the 9th International Symposium on Ferrocement (Ferro9), Bali* (pp. 305–318.

Jesse, F., Weiland, S., Curbach, M. (2005). Flexural strengthening of rc-structures with textile reinforced concrete, Textile Reinforced Concrete (TRC)—German/International Experience. ACI Special Publication, SP-250CD-4.

Kolsch, H. (1998). Carbon fiber cement matrix overlay system for masonry strengthening. *Journal of Composites for Construction, 2*(2), 105–109.

Lignola, G. P., Prota, A., & Manfredi, G. (2009). Nonlinear Analyses of tuff masonry walls strengthened with cementitious matrix grid composites. *Journal of Composites for Construction, 14*(4), 243–251.

Ombres, L. (2009). Failure modes in reinforced concrete beams strengthened with PBO fiber reinforced mortars. In *Proceedings of Fiber-Reinforced Polymer Reinforcement for Concrete Structures, FRPRCS-9, Sydney, Australia*.

Ombres, L. (2011). Flexural analysis of reinforced concrete beams strengthened with a cement based high strength composite material. *Composite Structures, 94*(1), 143–155.

Ombres, L. (2012). Debonding analysis of reinforced concrete beams strengthened with fibre reinforced cementitious mortar. *Engineering Fracture Mechanics, 81*, 94–109.

Ortlepp, R., Hampel, U., & Curbach, M. (2006). A new approach for evaluating bond capacity or TRC strengthening. *Cement & Concrete Composites, 28*, 589–597.

Ortlepp, R., Ortlepp, S., & Curbach, M. (2004). Stress transfer in the bond joint of subsequently applied Textile Reinforced Concrete strengthening. In *Proceedings of Fibre-Reinforced Concretes (FRC), RILEM, PRO 39, Varenna, Italy*.

Pareek, S., Suzuki, Y., & Kobayashi, A. (2007). Flexural and shear strengthening of RC beams using newly developed CFRP and polymer-cement pastes as bonding agents. In *Proceedings of Fiber-Reinforced Polymer Reinforcement for Concrete Structures, FRPRCS-8, Patras, Greece*.

Parisi, F., Lignola, G. P., Augenti, N., Prota, A., & Manfredi, G. (2011). Nonlinear Behavior of a Masonry Subassemblage Before and After Strengthening with Inorganic Matrix-Grid Composites. *Journal of Composites for Construction, 15*(5), 821–832.

Peled, A., Zaguri, E., & Marom, G. (2008). Bonding characteristics of multifilament polymer yarns and cement matrices. *Composites: Part A, 39*, 930–939.

Pellegrino, C., & D'Antino, T. (2013). Experimental behavior of existing precast prestressed reinforced concrete elements strengthened with cementitious composites. *Composites: Part B, 55*, 31–40.

Pellegrino, C., Tinazzi, D., & Modena, C. (2008). An experimental study on bond behavior between concrete and FRP reinforcement. *Journal of Compososites for Construction, 12*(2), 180–189.

Prota, A., Marcari, G., Fabbrocino, G., Manfredi, G., & Aldea, C. (2006). Experimental in-plane behavior of tuff masonry strengthened with cementitious matrix grid composites. *Journal of Composites for Construction, 10*(3), 223–233.

Smith, S. T., & Teng, J. G. (2002). FRP-strengthened RC beams-II: assessment of debonding strength models. *Engineering Structures, 24*(4), 397–417.

Sneed, L. H., D'Antino, T., & Carloni, C. (2014). Investigation of bond behavior of PBO fiber-reinforced cementitious matrix composite—concrete interface. *ACI Materials Journal, 111*(1–6), 1–12.

Sneed, L. H., D'Antino, T., Carloni, C., & Pellegrino, C. (2015). A comparison of the bond behavior of PBO-FRCM composites determined by single-lap and double-lap shear tests. *Cement and Concrete Composites*. doi:10.1016/j.cemconcomp.2015.07.007.

Soranakom, C., & Mobasher, B. (2009). Geometrical and mechanical aspects of fabric bonding and pullout in cement composites. *Materials and Structures, 42*, 765–777.

Subramaniam, K.V., Carloni, C., & Nobile, L. (2007). Width effect in the interface fracture during debonding of FRP from concrete. *Engineering Fracture Mechanics, 74*, 578–594.

Subramaniam, K.V., Carloni, C., & Nobile, L. (2011). An understanding of the width effect in FRP-concrete debonding. *Strain, 47*, 127–137.

Täljsten, B., & Blanksvärd, T. (2007). Mineral-Based bonding of Carbon FRP to strengthen concrete structures. *Journal of Composites for Construction, 11*(2), 120–128.

Triantafillou, T. C. (2010). Innovative Textile-based Composites for Strengthening and Seismic Retrofitting of Concrete and Masonry Structures. In *Proceedings of the 5th International Conference on FRP Composites in Civil Engineering, CICE-2010, Beijing, China*.

Triantafillou, T.C., Papanicolaou, C.G., Zissimopoulos, P., & Laourdekis, T. (2006). Concrete confinement with textile-reinforced mortar jackets. *ACI Structural Journal, 103*(1), 28–37.

UNI EN 1015-11. (2007). Methods of test for mortar for masonry—Part 11: Determination of flexural and compressive strength of hardened mortar, Comité Européen de Normalisation, Brussels, Belgium.

UNI EN 1998-3. (2005). Eurocode 8: Design of Structures for Earthquake Resistance—Part 3: Assessment and Retrofitting of Buildings, European Committee for Standardization, Brussels, Belgium.

Weiland, S., Ortlepp, R., & Curbach, M. (2006). Strengthening of preformed slabs with textile reinforced concrete. In *Proceedings of the 2nd International fib Congress, Naples, Italy*.

Wiberg, A. (2003). *Strengthening of Concrete Beams Using Cementitious Carbon Fibre Composites*. Doctoral Thesis, Royal Institute of Technology, Stockholm, Sweden.

Wu, H. C., & Sun, P. (2005). Fiber reinforced cement based composite sheets for structural retrofit. In *Proceedings of the International Symposium on Bond Behaviour of FRP in Structures, BBFS 2005, Hong Kong, China*.

Zastrau, B., Lepenies, I., & Richter. M. (2008). On the multi scale modeling of textile reinforced concrete. *Technische Mechanik, 28*, 53–63.